New Approach of Numerical Relativity:

Implementation, Tests and Applications

數值廣義相對論的新方法：

實施、測試和應用

LAM, Tsz-lok

林子樂

A Thesis Submitted in Partial Fulfilment
of the Reqirements for the Degree of
Master of Philosophy
in
Physics

The Chinese University of Hong Kong
July 2021

Thesis Assessment Committee

Professor Chu Ming Chung (Chair)

Professor Li Tjonnie Guang Feng (Thesis Supervisor)

Professor Ng Kenny Chun Yu (Committee Member)

Professor José Antonio Font (External Examiner)

Abstract

Many astrophysical scenarios involve neutron stars and black holes such as core-collapse supernovae, binary neutron star and neutron star-black hole mergers, which are the most important events in gravitational wave physics and multimessenger astrophysics. To numerically model these systems accurately within a reasonable time and affordable computational resources, a multi-scale, multi-dimensional, fully parallelized, support different geometries general relativistic (magneto-)hydrodynamics code is desired. We developed our new open-source, parallelized, block-grid adaptive, multi-dimensional general relativistic electro-magneto-hydrodynamics code `Gmunu` (General-relativistic multigrid numerical solver) in curvilinear geometries in dynamical spacetimes.
`Gmunu` code current adopts the conformal flatness condition approximation by solving the elliptic metric equations by multigrid approach. Although the `Gmunu` code pass with flying colors in benchmarking tests and demanding magnetohydrodynamics problems, the conformal flatness condition approximation prohibits the emission of gravitational wave in the simulation. Numerical simulations with full general-relativistic treatment are able to simulation gravitational wave signals emitted from various astrophysics events such as compact binary coalescence and core-collapse supernova. Therefore, it is necessary to extend our code to adopt the fully constrained formulation, which is a full general relativistic formulation naturally generalized from the conformal flatness condition approximation. In contrast to the fully hyperbolic formulations of general relativity such as BSSN and CCZ4, the fully constrained formulation maximizes the number of elliptic equations in each time steps by choosing maximal slicing condition and generalized Dirac gauge, leaving only two degrees of freedom in the hyperbolic sector which corresponds to the gravitational wave in far field regime. With the usage of multigrid solver, the elliptic metric equations can be solved multi-dimensionally in Cartesian, cylindrical or spherical geometries.
We present the methodology, implementation details and the performance of the fully constrained formulation in `Gmunu`.

摘要

許多天體物理場景都涉及中子星和黑洞，例如核心坍縮超新星、雙中子星和中子星-黑洞合併，它們是引力波物理學和多信使天體物理學中最重要的事件。爲了在合理的時間和負擔得起的計算資源內準確地對這些系統進行數值模擬，需要多尺度、多維、完全並行、支持不同幾何形狀的通用相對論（磁）流體動力學代碼。我們開發了新的開源、並行化、塊網格自適應、多維廣義相對論電磁流體動力學代碼豬緲妞（廣義相對論多重網格數值求解器），用於動態時空曲線幾何。

豬緲妞 碼流採用共形平坦度條件近似，通過多重網格方法求解橢圓度量方程。儘管豬緲妞 代碼在基準測試和苛刻的磁流體動力學問題中表現出色，但保形平坦度條件近似阻止了模擬中引力波的發射。具有完全廣義相對論處理的數值模擬能夠模擬從各種天體物理事件發出的引力波信號，例如緻密二元聚結和核心坍縮超新星。因此，有必要擴展我們的代碼以採用完全約束公式，這是從保角平坦度條件近似自然推廣的完全廣義相對論公式。與廣義相對論的全雙曲公式相比，全約束公式通過選擇最大切片條件和廣義狄拉克規範，在每個時間步中最大化橢圓方程的數量，雙曲扇區只留下兩個自由度這對應於遠場區域的引力波。使用多重網格求解器，橢圓度量方程可以在笛卡爾、圓柱或球面幾何中進行多維求解。

我們介紹了豬緲妞 中完全約束公式的方法、實現細節和性能。

Conventions and Units

Unless explicitly stated, we adopt the geometrized Heaviside-Lorentz units, for which the speed of light c, gravitational constant G, solar mass $M_\odot$, vacuum permittivity ϵ_0 and vacuum permeability μ_0 are all equal to one ($c = G = M_\odot = \epsilon_0 = \mu_0 = 1$). Greek indices (e.g. $\mu, \nu, \rho, \sigma, \dots$), running from 0 to 3, are used for 4-quantities while the Roman indices (e.g. $i, j, k, \dots$), running from 1 to 3, are used for 3-quantities.

Table of contents

List of figures

List of tables

Part I

Methodology: Formulations

Chapter 1

Formulations of Einstein Field Equations

1.1 Introduction to general relativity

1.1.1 Einstein field equations

The Einstein field equations is given by

$$G_{\mu\nu} = 8\pi T_{\mu\nu}, \tag{1.1}$$

where $T_{\mu\nu}$ is the enery-momentum tensor and $G_{\mu\nu}$ is the Einstein tensor. The Einstein tensor $G_{\mu\nu}$ is defined as

$$G_{\mu\nu} \coloneqq R_{\mu\nu} - \frac{1}{2} g_{\mu\nu} R, \tag{1.2}$$

where $R_{\mu\nu}$ is the Ricci tensor, R is the Ricci scalar and $g_{\mu\nu}$ is the metric tensor.

1.2 The 3+1 decomposition of spacetime

Due to the complexity and nonlinearity of Einstein field equations, it is extremely difficult to obtain analytical solution even for the simplest dynamical evolution systems. Therefore, the accurate discription of the such systems can only be derived through numerical simulation. For this, we need to reformulate the Einstein equations as an initial-value problem or Cauchy problem. In this chapter, we will introduction the Arnowitt-Deser-

Misner (ADM) formulation, which is one of the milestone of 3+1 numerical relativity. In particular, we will focus on the constrained evolution scheme for the Einstein equations. For more comprehensive discussion of numerical relativity, we refer readers to [6, 34, 61].

1.2.1 Foliation of spacetime

In the 3+1 decomposition, the spacetime manifold $\mathcal{M}$ is foliated into a set of non-intersecting spacelike hypersurfaces Σ_t parameterized by the coordinate time t [46]. We denote a future-directed timelike unit four-vector n^μ normal to the hypersurface Σ_t (i.e. $n_\mu \propto \nabla_\mu t$). The induced spacetime metric $\gamma_{\mu\nu}$ on each hypersurfuce can then be defined as

$$\gamma_{\mu\nu} \coloneqq g_{\mu\nu} + n_\mu n_\nu. \tag{1.3}$$

Thus, we can construct spatial projection tensor $\gamma^\mu{}_\nu$ and time projection tensor $N^\mu{}_\nu$ as

$$\gamma^\mu{}_\nu \coloneqq \delta^\mu{}_\nu + n^\mu n_\nu, \qquad N^\mu{}_\nu \coloneqq -n^\mu n_\nu, \tag{1.4}$$

which decompose any generic four-vector U^μ into spatial part $\gamma^\mu{}_\nu U^\nu$ and timelike part $N^\mu{}_\nu U^\nu$. Therefore, we can decompose the timelike vector field

$$t^\mu = \alpha n^\mu + \beta^\mu \tag{1.5}$$

into two components as

$$\alpha \coloneqq -t^\mu n_\mu, \qquad \beta^\mu \coloneqq t^\nu \gamma^\mu{}_\nu, \tag{1.6}$$

where the lapse function α measures the physical proper time ($\alpha\Delta t$) between two neighboring spatial hypersurface Σ_t and $\Sigma_{t+\Delta t}$, and the shift vector β^i measures the changes of spatial coordinates on $\Sigma_{t+\Delta t}$.
Here, we summarise several useful relations. The timelike normal vector n^μ and its corresponding one-form n_μ can be expressed as

$$n^\mu = \frac{1}{\alpha}\left(1, \beta^i\right), \qquad n_\mu = \left(\alpha, \vec{0},\right). \tag{1.7}$$

The generic line element in 3+1 decomposition is given by

$$ds^2 = -\left(\alpha^2 - \beta^i\beta_i\right)dt^2 + \beta_i dx^i dt + \gamma_{ij} dx^i dx^j \tag{1.8}$$

The covariant and contravariant components of the metric can be written as

$$g_{\mu\nu} = \begin{pmatrix} -\alpha^2 + \beta^i\beta_i & \beta_j \\ \beta_i & \gamma_{ij} \end{pmatrix}, \qquad g^{\mu\nu} = \begin{pmatrix} -\frac{1}{\alpha^2} & \frac{\beta^j}{\alpha^2} \\ \frac{\beta^i}{\alpha^2} & \gamma^{ij} - \frac{\beta^i\beta^j}{\alpha^2} \end{pmatrix}. \tag{1.9}$$

From equation(1.9), we can conclude that

$$\sqrt{-g} = \alpha\sqrt{\gamma}, \tag{1.10}$$

where $g \coloneqq \det(g_{\mu\nu})$ and $\gamma \coloneqq \det(\gamma_{ij})$.

1.2.2 Derivative operator

With the 3+1 decomposition, we can now construct the 3-dimensional covariant derivative D_α associated with $\gamma_{\mu\nu}$ by projecting the 4-dimensional covariant derivative ∇_α onto Σ_t, which is given by

$$D_\alpha T^{\mu_1\mu_2\cdots}{}_{\nu_1\nu_2\ldots} = \gamma_\alpha{}^\beta \gamma_{\rho_1}{}^{\mu_1}\gamma_{\rho_2}{}^{\mu_2}\ldots\gamma_{\nu_1}{}^{\sigma_1}\gamma_{\nu_2}{}^{\sigma_2}\ldots\nabla_\beta T^{\rho_1\rho_2\cdots}{}_{\sigma_1\sigma_2\ldots}, \tag{1.11}$$

for arbitrary tensor $T^{\mu_1\mu_2\cdots}{}_{\nu_1\nu_2\ldots}$ on spatial hypersurface Σ_t. Using equation(1.11), it can be shown that the corvariant derivative of $\gamma_{\mu\nu}$ vanishes

$$\begin{aligned} D_\alpha\gamma_{\mu\nu} &= \gamma_\alpha{}^\beta\gamma_\rho{}^\mu\gamma_\nu{}^\sigma\nabla_\beta\left(g_{\rho\sigma} + n_\rho n_\sigma\right) \\ &= \gamma_\alpha{}^\beta\gamma_\rho{}^\mu\gamma_\nu{}^\sigma\left(n_\rho\nabla_\beta n_\sigma + n_\sigma\nabla_\beta n_\rho\right) = 0 \end{aligned} \tag{1.12}$$

The components of 3-dimensional connection coefficients $\Gamma^\alpha{}_{\mu\nu}$ in coordinate basis can be expressed as

$$\Gamma^\alpha{}_{\mu\nu} = \frac{1}{2}\gamma^{\alpha\beta}\left(\partial_\nu\gamma_{\beta\mu} + \partial_\mu\gamma_{\beta\nu} - \partial_\beta\gamma_{\mu\nu}\right). \tag{1.13}$$

Here, the upper left index ${}^{(4)}$ marks the 4-dimensional tensors while the unmarked one represents purely spatial 3-dimensional tensors. Similarly, the 3-dimensional Riemann tensor $R^\alpha{}_{\beta\mu\nu}$ associated with $\gamma_{\mu\nu}$ is defined by requiring that

$$D_\nu D_\mu W_\beta - D_\mu D_\nu W_\beta = W_\alpha R^\alpha{}_{\beta\mu\nu}, \qquad R^\alpha{}_{\beta\mu\nu}n_\alpha = 0, \tag{1.14}$$

which can be explicitly expressed in coordinate basis as

$$R^{\alpha}{}_{\beta\mu\nu} = \partial_\mu \Gamma^{\alpha}{}_{\beta\nu} - \partial_\nu \Gamma^{\alpha}{}_{\beta\mu} + \Gamma^{\alpha}{}_{\mu\rho}\Gamma^{\rho}{}_{\beta\nu} - \Gamma^{\alpha}{}_{\nu\rho}\Gamma^{\rho}{}_{\beta\mu}. \tag{1.15}$$

The 3-dimensional Ricci tensor $R_{\mu\nu}$ and Ricci scalar R are defined in a similar manner as their 4-dimensional counterparts

$$R_{\mu\nu} \coloneqq R^{\alpha}{}_{\mu\alpha\nu}, \qquad\qquad R \coloneqq R^{\mu}{}_{\mu}. \tag{1.16}$$

Since $R^{\alpha}{}_{\beta\mu\nu}$ is purely spatial and can be computed by the spatial derivatives of the spatial metric alone, it only contains about information about the curvature intrinsic to the hypersurface Σ_t, but cannot contain all the information of ${}^{(4)}R^{\alpha}{}_{\beta\mu\nu}$ which includes time derivative of the 4-dimensional metric. The missing information can be found in a purely spatial symmetric tensor called the extrinsic curvature $K_{\mu\nu}$.

1.2.3 Extrinsic curvature

The extrinsic curvature $K_{\mu\nu}$ is related to the time derivative of the spatial metric $\gamma_{\mu\nu}$. Therefore, the spatial metric and extrinsic curvature $(\gamma_{\mu\nu}, K_{\mu\nu})$ are equivalent to the positions and velocities in classical mechanics, which describe the instantaneous state of the gravitational field. It can be obtained by projecting of the gradient of the normal vector $\gamma_\mu{}^\lambda \gamma_\nu{}^\rho \nabla_\lambda n_\rho$ into the hypersurface Σ_t, and then taking the negative expression of the symmetric part

$$\begin{aligned} K_{\mu\nu} &\coloneqq -\gamma_\mu{}^\lambda \gamma_\nu{}^\rho \nabla_\lambda n_\rho \\ &= -\gamma_\mu{}^\lambda \left(\delta_\nu{}^\rho + n_\nu n^\rho\right) \nabla_\lambda n_\rho \\ &= -\gamma_\mu{}^\lambda \nabla_\lambda n_\nu, \end{aligned} \tag{1.17}$$

where the identity $n^\rho \nabla_\lambda n_\rho = 0$ is used.
We can also define an spatial acceleration a_ν

$$a_\nu \coloneqq n^\mu \nabla_\mu n_\nu, \tag{1.18}$$

satisfying the identities

$$a_\nu = D_\nu \ln \alpha, \tag{1.19}$$

to rewrite equation(1.17) as

$$K_{\mu\nu} = -\nabla_\mu n_\nu - n_\mu a_\nu \tag{1.20}$$

Finally, we can write the extrinsic curvature $K_{\mu\nu}$ as the Lie derivative of the spatial metric along the local normal n^μ

$$K_{\mu\nu} = -\frac{1}{2}\mathcal{L}_n \gamma_{\mu\nu}. \tag{1.21}$$

Using equation(1.5), we can express the Lie derivative $\mathcal{L}_n$ as

$$\mathcal{L}_n = \frac{1}{\alpha}\left(\mathcal{L}_t - \mathcal{L}_\beta\right), \tag{1.22}$$

and thus obtain the evolution equation for the spatial metric

$$\mathcal{L}_t \gamma_{\mu\nu} = -2\alpha K_{\mu\nu} + \mathcal{L}_\beta \gamma_{\mu\nu}. \tag{1.23}$$

1.2.4 The Gauss, Codazzi and Ricci equations

To express the Einstein field equations in term of the spatial variables $(\gamma_{\mu\nu}, K_{\mu\nu})$ we defined previously, we first need to relate 3-dimensional Riemann tensor ${R^\alpha}_{\beta\mu\nu}$ on Σ_t to the 4-dimensional Riemann tensor ${}^{(4)}{R^\alpha}_{\beta\mu\nu}$ on $\mathcal{M}$, The relation between ${R^\alpha}_{\beta\mu\nu}$ and the full spatial projection of ${}^{(4)}{R^\alpha}_{\beta\mu\nu}$ is given by the *Gauss' equation*

$$R_{\alpha\beta\mu\nu} + K_{\alpha\mu}K_{\beta\nu} - K_{\alpha\nu}K_{\beta\mu} = {\gamma_\alpha}^\rho {\gamma_\beta}^\sigma {\gamma_\mu}^\lambda {\gamma_\nu}^{\delta\,(4)}R_{\rho\sigma\lambda\delta}, \tag{1.24}$$

while the projection of ${}^{(4)}{R^\alpha}_{\beta\mu\nu}$ with one index projected in the normal direction is given by the *Codazzi equation*

$$D_\nu K_{\mu\alpha} - D_\mu K_{\nu\alpha} = {\gamma_\mu}^\rho {\gamma_\nu}^\sigma {\gamma_\alpha}^\lambda n^{\delta\,(4)}R_{\rho\sigma\lambda\delta}. \tag{1.25}$$

Finally, by projecting two indices of ${}^{(4)}R_{\rho\sigma\lambda\delta}$ in the normal direction, we can relate it to the time derivative of $K_{\mu\nu}$

$$\mathcal{L}_n K_{\mu\nu} = n^\alpha n^\beta {\gamma_\mu}^\lambda {\gamma_\nu}^{\delta\,(4)}R_{\alpha\beta\lambda} - \frac{1}{\alpha}D_\mu D_\nu \alpha - {K_\nu}^\lambda K_{\mu\lambda}, \tag{1.26}$$

which is called the *Ricci equation*.

1.2.5 Constraint and evolution equations

Using the Gauss, Codazzi and Ricci equations, the Einstein fields equations can be decomposed into a set of evolution equations and a set of constraint equations of $(\gamma_{\mu\nu}, K_{\mu\nu})$. To begin with, we define the following matter quantities

$$S_{\mu\nu} :=\gamma^{\alpha}{}_{\mu}\gamma^{\beta}{}_{\nu}T_{\alpha\beta}, \tag{1.27}$$
$$S_{\mu} :=-\gamma^{\alpha}{}_{\mu}n^{\beta}T_{\alpha\beta}, \tag{1.28}$$
$$S :=S^{\mu}{}_{\mu}, \tag{1.29}$$
$$E :=n^{\alpha}n^{\beta}T_{\alpha\beta}, \tag{1.30}$$

which decompose the stress-energy tensor as

$$T_{\mu\nu} = En_{\mu}n_{\nu} + S_{\mu}n_{\nu} + S_{\nu}n_{\mu} + S_{\mu\nu}. \tag{1.31}$$

By contracting the α, μ indices in equation(1.24), we can obtain

$$R_{\mu\nu} = \gamma_{\mu}{}^{\alpha}\gamma_{\nu}{}^{\beta}\left({}^{(4)}R_{\alpha\beta} + n^{\rho}n^{\sigma}{}^{(4)}R_{\alpha\rho\beta\sigma}\right) + K_{\mu\lambda}K_{\nu}{}^{\lambda} - K_{\mu\nu}K, \tag{1.32}$$

where $K \coloneqq K^{\mu}{}_{\mu}$ is the trace of the extrinsic curvature, called the *mean curvature*. Further contracting the μ, ν indices in equation(1.32), the contracted Gauss' equation becomes

$$2n^{\mu}n^{\nu}G_{\mu\nu} = R + K^2 - K_{\mu\nu}K^{\mu\nu}, \tag{1.33}$$

Using the Einstein equation(1.1), we can obtain the *Hamiltonian constraint*

$$R + K^2 - K_{\mu\nu}K^{\mu\nu} = 16\pi E. \tag{1.34}$$

Similarly, by contracting α, ν indices in equation(1.25), the Codazzi equation yields

$$D_{\nu}K_{\mu}{}^{\nu} - D_{\mu}K = -8\pi\gamma^{\alpha}{}_{\mu}n^{\beta}T_{\alpha\beta}, \tag{1.35}$$

and thus obtain the *momentum constrain equation*

$$D_{\nu}K_{\mu}{}^{\nu} - D_{\mu}K = 8\pi S_{\mu}. \tag{1.36}$$

The Ricci equation (1.26) can be rewritten using equation(1.32) to

$$\mathcal{L}_n K_{\mu\nu} = R_{\mu\nu} - \gamma_\mu{}^\rho \gamma_\nu{}^{\sigma\,(4)} R_{\rho\sigma} - 2K_{\mu\lambda}K_\nu{}^\lambda + KK_{\mu\nu} - \frac{1}{\alpha} D_\mu D_\nu \alpha. \tag{1.37}$$

Using the Einstein equations (1.1)

$$\begin{aligned} \gamma_\mu{}^\rho \gamma_\nu{}^{\sigma\,(4)} R_{\rho\sigma} &= 8\pi \gamma_\mu{}^\rho \gamma_\nu{}^\sigma \left(T_{\rho\sigma} - \frac{1}{2} g_{\rho\sigma} T^\mu{}_\mu \right) \\ &= 8\pi \left[S_{\mu\nu} - \frac{1}{2} \gamma_{\mu\nu} \left(S - E \right) \right] \end{aligned} \tag{1.38}$$

and equation(1.22), we can finally obtain the evolution equation for $K_{\mu\nu}$ as

$$\mathcal{L}_t K_{\mu\nu} = -D_\mu D_\nu \alpha + \alpha \left(R_{\mu\nu} - 2K_{\mu\lambda}K_\nu{}^\lambda + KK_{\mu\nu} \right) - 8\pi\alpha \left[S_{\mu\nu} - \frac{1}{2} \gamma_{\mu\nu} \left(S - E \right) \right] + \mathcal{L}_\beta K_{\mu\nu}. \tag{1.39}$$

1.2.6 The Arnowitt, Deser and Misner equations

The Lie derivative in the evolution equations (1.23) and (1.39) can be expressed in terms of coordinate basis as

$$\mathcal{L}_t K_{\mu\nu} = \partial_t K_{\mu\nu} \tag{1.40}$$

$$\mathcal{L}_\beta K_{\mu\nu} = \beta^\lambda D_\lambda K_{\mu\nu} + K_{\mu\lambda} D_\nu \beta^\lambda + K_{\lambda\nu} D_\mu \beta^\lambda \tag{1.41}$$

As the result, the Einstein field equaitons (1.1) in the standard 3+1 decomposition can be decomposed into a set of constraint equations and evolution equation of (γ_{ij}, K_{ij}) in terms of coordinate basis, which are referred to as the Arnowitt, Deser and Misner (ADM)

equations [1, 84]

$$R + K^2 - K_{ij}K^{ij} = 16\pi E, \qquad \text{(Hamiltonian constraint)} \tag{1.42}$$

$$D_j\left(K^{ij} - \gamma^{ij}K\right) = 8\pi S^i, \qquad \text{(momentum constraint)} \tag{1.43}$$

$$\partial_t \gamma_{ij} = -2\alpha K_{ij} + D_i\beta_j + D_j\beta_i, \qquad \text{(spatial metric evolution)} \tag{1.44}$$

$$\begin{aligned}\partial_t K_{ij} = &- D_iD_j\alpha + \alpha\left(R_{ij} - 2K_{ik}K_j{}^k + KK_{ij}\right)\\ &- 8\pi\alpha\left[S_{ij} - \frac{1}{2}\gamma_{ij}\left(S - E\right)\right]\\ &+ \beta^k D_k K_{ij} + K_{ik}D_j\beta^k + K_{kj}D_i\beta^k.\end{aligned} \qquad \text{(extrinsic curvature evolution)} \tag{1.45}$$

1.3 Conformal Decomposition

The conformal decompostion factors out a scalar component from a spatial metric. It was first developped for initial data problems in general relativity [44, 82, 83, 85], and then used in reformulating evolution equations in the 3+1 formulation. In this section, we will discuss the conformal decomposition of spatial metric and extrinsic curvature in numerical relativity.

1.3.1 Conformal transformation of the spatial metric

We consider the conformal transformation of the spatial metric γ_{ij} as

$$\tilde{\gamma}_{ij} = \psi^{-4}\gamma_{ij}, \tag{1.46}$$

where $\tilde{\gamma}_{ij}$ is the *conformal metric* and ψ is a positive scaling factor satisfying

$$\psi \coloneqq \det\left(\frac{\gamma}{f}\right), \qquad \gamma \coloneqq \det\left(\gamma_{ij}\right), \qquad f \coloneqq \det\left(f_{ij}\right) \tag{1.47}$$

for a time independent flat metric f_{ij} (i.e. $\det\left(\tilde{\gamma}_{ij}\right) = f$ by construction).
Thus, the *inverse conformal metric* is given by

$$\tilde{\gamma}^{ij} \coloneqq \psi^4\gamma^{ij}. \tag{1.48}$$

Substituting the conformal transformation (1.46) into equation(1.13), we can obtain the transformation law for 3-dimensional connection coefficient

$$\Gamma^i{}_{jk} = \tilde{\Gamma}^i{}_{jk} + 2\left(\delta^i{}_j \tilde{D}_k \ln\psi + \delta^i{}_k \tilde{D}_j \ln\psi - \tilde{\gamma}_{jk}\tilde{\gamma}^{il}\tilde{D}_l \ln\psi\right). \tag{1.49}$$

From now on, we denote all objects associated with the conformal metric $\tilde{\gamma}^{ij}$ with a tilde symbol. Similarly, the transformation for Ricci tensor and scalar curvature are given by

$$\begin{aligned} R_{ij} =& \tilde{R}_{ij} - 2\left(\tilde{D}_i\tilde{D}_j \ln\psi + \tilde{\gamma}_{ij}\tilde{\gamma}^{lm}\tilde{D}_l\tilde{D}_m \ln\psi\right) \\ &+ 4\left[\left(\tilde{D}_i \ln\psi\right)\left(\tilde{D}_j \ln\psi\right) - \tilde{\gamma}_{ij}\tilde{\gamma}^{lm}\tilde{D}_l\left(\tilde{D}_l \ln\psi\right)\left(\tilde{D}_m \ln\psi\right)\right] \end{aligned} \tag{1.50}$$

$$R = \psi^{-4}\tilde{R} - 8\psi^{-5}\tilde{D}^2\psi, \tag{1.51}$$

where $\tilde{D}^2 = \tilde{\gamma}^{ij}\tilde{D}_i\tilde{D}_j$ denotes the Laplace operator associated with $\tilde{\gamma}_{ij}$. Therefore, using equation(1.51), the Hamiltonian constraint (1.42) becomes

$$8\tilde{D}^2\psi - \psi\tilde{R} - \psi^5 K^2 + \psi^2 K_{ij}K^{ij} = -16\pi\psi^5 E. \tag{1.52}$$

1.3.2 Conformal transformation of the extrinsic curvature

Traceless decomposition

Before we perform the conformal transformation to the extrinsic curvature K_{ij}, it is convenient to split K_{ij} into the trace part

$$K \coloneqq \gamma^{ij}K_{ij}, \tag{1.53}$$

and its traceless part

$$A_{ij} \coloneqq K_{ij} - \frac{1}{3}\gamma_{ij}K, \qquad \mathrm{tr}_\gamma\, A_{ij} = \gamma^{ij}A_{ij} = 0. \tag{1.54}$$

Therefore, we can obtain the tracelss decomposition of the extrinsic curvature

$$K_{ij} = A_{ij} + \frac{1}{3}\gamma_{ij}K, \qquad K^{ij} = A^{ij} + \frac{1}{3}\gamma^{ij}K. \tag{1.55}$$

The evolution equations of the spatial metric (1.44) in conformal decomposition formulation can hence be written as

$$\partial_t \psi = \beta^i \tilde{D}_i \psi - \frac{1}{6}\psi \left(\alpha K - \tilde{D}_i \beta^i\right), \qquad \text{(conformal factor evolution)} \tag{1.56}$$

$$\partial_t \tilde{\gamma}_{ij} = -2\alpha\psi^{-4} A_{ij} + \tilde{\gamma}_{jk}\tilde{D}_i\beta^k + \tilde{\gamma}_{ik}\tilde{D}_j\beta^k - \frac{2}{3}\tilde{\gamma}_{ij}\tilde{D}_k\beta^k, \qquad \text{(conformal metric evolution)} \tag{1.57}$$

and the constraint equations become

$$\tilde{D}^2\psi - \frac{1}{8}\psi\tilde{R} + \left(\frac{1}{8}A_{ij}A^{ij} - \frac{1}{12}K^2 + 2\pi E\right)\psi^5 = 0, \qquad \text{(Hamiltonian constraint)} \tag{1.58}$$

$$\tilde{D}_j\left(\psi^{10}A^{ij}\right) - \frac{2}{3}\psi^6\tilde{D}^i K = 8\pi\psi^{10}S^i. \qquad \text{(momentum constraint)} \tag{1.59}$$

Conformal transformation of the traceless part

We consider the transformation

$$A^{ij} := \psi^a \tilde{A}^{ij}, \tag{1.60}$$

for some undetermined exponent α. Here, we discuss two natural choices of a: $a = -4$ and $a = -10$.

"Time-evolution" scaling: $a = -4$. This choice of scaling was considered by Nakamura in 1994 [49], It comes naturally from the evolution equation of conformal metric (1.57), where the $\psi^{-4}A_{ij}$ term suggests the conformal transformation of A_{ij} to have the same scaling factor as the conformal spatial metric (1.48)

$$\tilde{A}^{ij} := \psi^4 A^{ij}, \tag{1.61}$$

where the indices of $\tilde{A}^{ij}$ and $\tilde{A}_{ij}$ are lowered and raised by the conformal metric $\tilde{\gamma}_{ij}$ and $\tilde{\gamma}^{ij}$ respectively (i.e. $\tilde{A}_{ij} = \tilde{\gamma}_{il}\tilde{\gamma}_{jm}\tilde{A}^{lm} = \psi^{-4}A_{ij}$). The evolution equations of conformal spatial metric therefore become

$$\partial_t \tilde{\gamma}_{ij} = -2\alpha\tilde{A}_{ij} + \tilde{\gamma}_{jk}\tilde{D}_i\beta^k + \tilde{\gamma}_{ik}\tilde{D}_j\beta^k - \frac{2}{3}\tilde{\gamma}_{ij}\tilde{D}_k\beta^k. \tag{1.62}$$

The Hamiltonian constraint and momentum constraint in this scaling is rewritten as

$$\tilde{D}^2\psi = \frac{1}{8}\psi\tilde{R} - \left(2\pi E - \frac{1}{12}K^2 + \frac{1}{8}\tilde{A}_{ij}\tilde{A}^{ij}\right)\psi^5, \tag{1.63}$$

$$\tilde{D}_j\left(\psi^6\tilde{A}^{ij}\right) - \frac{2}{3}\psi^6\tilde{D}^iK = 8\pi\psi^{10}S^i. \tag{1.64}$$

"Momentum-constraint" scaling: $a = -10$. Another possible choice of scaling factor $a = -10$ originates from the momentum constraint equation (1.59), which was first suggested by Lichnerowicz in 1944 [44]. we define

$$\hat{A}^{ij} \coloneqq \psi^{10}A^{ij}, \tag{1.65}$$

and thus

$$\hat{A}_{ij} = \psi^2 A_{ij}. \tag{1.66}$$

Here, we use hat symbol to separate the "momentum-constraint" scaling from the tilde symbol in "time-evolution" scaling. These two scaling are related by

$$\hat{A}^{ij} = \psi^6\tilde{A}^{ij}, \qquad \hat{A}_{ij} = \psi^6\tilde{A}_{ij}, \qquad \hat{A}_{ij}\hat{A}^{ij} = \psi^{12}\tilde{A}_{ij}\tilde{A}^{ij} \tag{1.67}$$

Therefore, the constraint equations can be written as

$$\tilde{D}^2\psi = \frac{1}{8}\psi\tilde{R} - \left(2\pi E - \frac{1}{12}K^2\right)\psi^5 - \frac{1}{8}\hat{A}_{ij}\hat{A}^{ij}\psi^{-7}, \tag{1.68}$$

$$\tilde{D}_i\hat{A}^{ij} - \frac{2}{3}\psi^6\tilde{D}^iK = 8\pi\psi^{10}S^i. \tag{1.69}$$

Equation(1.69) is known as *Lichnerowicz equation*. Although equation (1.64) and equation (1.69) are equivalent, they have different mathematical properties if they are treated as a partial differential equation for ψ. According to the maximal principle, the local uniqueness of the solutions depends on the sign of the exponent of ψ in the quadratic extrinsic curvature A^2 term [26, 32, 56, 68, 71]. Equation (1.63) suffers from the mathematical nonuniqueness problems due to the positive exponent $(+5)$, while the negative exponent (-7) in equation (1.68) guarantees the local uniquess of the solutions.

1.3.3 Conformal transverse-traceless decomposition

Using the "momentum-constraint" scaling mentioned previously, we can further decompose the symmetric, traceless tensor $\hat{A}^{ij}$ as

$$\hat{A}^{ij} = \hat{A}^{ij}_{TT} + \hat{A}^{ij}_{L}, \tag{1.70}$$

where $\hat{A}^{ij}_{TT}$ is the transverse-traceless part which is divergenceless

$$\tilde{D}_j \hat{A}^{ij}_{L} = 0, \tag{1.71}$$

and $\hat{A}^{ij}_{L}$ is the longitudinal part satisfying

$$\hat{A}^{ij}_{L} = \tilde{D}^i X^j + \tilde{D}^j X^i - \frac{2}{3}\tilde{\gamma}^{ij}\tilde{D}_k X^k \equiv \left(\tilde{L}X\right)^{ij}. \tag{1.72}$$

The vector X^i here is the vector potential and $\tilde{L}$ is the *longitudinal operator* or *conformal Killing operator* associated with $\tilde{\gamma}$ which gives a symmetric, traceless tensor. The divergence of $\hat{A}^{ij}$ becomes

$$\tilde{D}_j \hat{A}^{ij} = \tilde{D}^2 X^i + \frac{1}{3}\tilde{D}^i\left(\tilde{D}_j X^j\right) + \tilde{R}^i{}_j X^j \equiv \tilde{\Delta}_L, \tag{1.73}$$

where $\tilde{\Delta}_L$ is the *vector Laplacian*. Thus, the momentum constraint in the conformal transverse-traceless (CTT) decomposition yields

$$\tilde{\Delta}_L X^i - \frac{2}{3}\psi^6 \tilde{D}^i K = 8\pi\psi^{10} S^i, \tag{1.74}$$

and the corresponding Hamiltonian constraint is the same as equation (1.68).

1.4 Gauge Condition

In the 3+1 formulation of spacetime, the gauge freedom is preserved. One can freely choose the lapse function α and shift vector β^i. In this section, we introduce the *maximal slicing* condition and *generalized Dirac gauge*, which is used in the formulation of the constrained scheme in the next section.

1.4.1 Maximal Slicing

By taking the trace of the evolution equation for extrinsic curvature (1.45), we can obtain an elliptic equation for the lapse α

$$D^2\alpha = -\partial_t K + \alpha\left[K_{ij}K^{ij} + 4\pi\left(E+S\right)\right] + \beta^i D_i K. \tag{1.75}$$

One well-known choice to further simplify this equation is the *maximal slicing* condition

$$K = 0 = \partial_t K, \tag{1.76}$$

which corresponds to the vanishing mean curvature in all hypersurface Σ_t. This type of slicing was first introduced by Lichnerowicz [44] and then made popularized by York [68, 69]. Under this condition, the enclosed volume inside some hypersurface Σ_t becomes maximal, hence the name *maximal slicing*. With this choice of condition, equation (1.75) reduces to

$$D^2\alpha = \alpha\left[A_{ij}A^{ij} + 4\pi\left(E+S\right)\right], \tag{1.77}$$

which is independent of the shift β^i. Alternatively, we can combine the conformally decomposed Hamiltonian equation (1.68) to obtain

$$\tilde{D}^2\left(\alpha\psi\right) = \alpha\psi\left[\frac{7}{8}\psi^{-8}\hat{A}_{ij}\hat{A}^{ij} + \frac{1}{8}\tilde{R} + 2\pi\psi^4\left(E+2S\right)\right]. \tag{1.78}$$

The *maximal slicing* condition not only helps decouple the constraint equations, but also has some nice physical properties: it is a natural extension of Newtonian gravity and has singularity avoidance property.

Natural generalization to Newtonian limit

Consider the Newtonain limit of a weak and static gravitational field

$$\alpha \approx 1+\Phi, \qquad \gamma_{ij} \approx \left(1+2\Phi\right) f_{ij}, \qquad K_{ij} = 0, \qquad \text{for } \Phi \ll 1, \tag{1.79}$$

where Φ is the Newtonian gravitational potential, and non-relativistic matter

$$S \ll E, \qquad E \approx \rho_0, \tag{1.80}$$

where ρ_0 is the proper rest mass energy density. Equation (1.77) reduces to Poisson equation for the newtonian gravitational potential

$$\nabla^2\Phi = 4\pi\rho_0. \tag{1.81}$$

Singularity avoidance

Another interesting property of maximal slicing is singularity avoidance. Equation (1.17) shows that under maximal slicing condition, the normal observers move like irrotational and incompressible fluid elements

$$\nabla_\mu n^\mu = 0, \tag{1.82}$$

which implies that focusing of the timelike unit normal vector field is prohibited. It can also be seen from equation (1.44), which yields the following continuity equation for volume element $\sqrt{\gamma}$ in maximal slicing condition

$$\partial_t\sqrt{\gamma} = \partial_i\left(\sqrt{\gamma}\beta^i\right). \tag{1.83}$$

This suggests that as long as a regular shift vector is chosen and the initial condition for $\gamma_{\mu\nu}$ is regular, γ is regular forever.

1.4.2 Generalized Dirac Gauge

The *Dirac gauge* was first introduced by Dirac in 1959 [31], and then generalized by the Meudon group [12]. We define the *generalized Dirac gauge* as

$$\mathcal{D}_j\tilde{\gamma}^{ij} = 0, \tag{1.84}$$

which fully specify the coordinates in the hypersurface Σ_t including the initial one. Here, $\mathcal{D}$ denotes the covariant derivative associated with the flat background metric f_{ij} defined in equation (1.47), which relates $\tilde{D}$ by

$$\tilde{D}_k T^{i_1\ldots i_p}{}_{j_1\ldots j_q} = \mathcal{D}_k T^{i_1\ldots i_p}{}_{j_1\ldots j_q} + \sum_{r=1}^{p}\Delta^{i_r}{}_{lk}T^{i_1\ldots l\ldots i_p}{}_{j_1\ldots j_q} + \sum_{r=1}^{q}\Delta^{l}{}_{j_r k}T^{i_1\ldots i_p}{}_{j_1\ldots l\ldots j_q}, \tag{1.85}$$

where $\Delta^k{}_{ij}$ is given by

$$\Delta^k{}_{ij} \coloneqq \frac{1}{2}\tilde{\gamma}^{kl}\left(\mathcal{D}_i\tilde{\gamma}_{lj} + \mathcal{D}_j\tilde{\gamma}_{il} - \mathcal{D}_l\tilde{\gamma}_{ij}\right). \tag{1.86}$$

We can further define the potentials h^{ij} as the deviation of the conformal metric from the flat fiducial metric

$$h^{ij} \coloneqq \tilde{\gamma}^{ij} - f^{ij}. \tag{1.87}$$

Thus, the generalized Dirac is equivalent to

$$\mathcal{D}_j h^{ij} = 0, \tag{1.88}$$

Under such gauge condition, the conformal Ricci tensor $\tilde{R}^{ij}$ is simplified drastically as

$$\tilde{R}^{ij} = \frac{1}{2}\mathcal{D}^2 h^{ij} + \tilde{R}^{ij}_*, \tag{1.89}$$

where $\tilde{R}^{ij}_*$ is the quadratic part of $\tilde{R}^{ij}$

$$\tilde{R}^{ij}_* \coloneqq \frac{1}{2}\Bigg[h^{kl}\mathcal{D}_k\mathcal{D}_l h^{ij} - \mathcal{D}_l h^{ik}\mathcal{D}_k h^{jl} - \tilde{\gamma}_{kl}\tilde{\gamma}^{mn}\mathcal{D}_m h^{ik}\mathcal{D}_n h^{jl} \tag{1.90}$$

$$+ \tilde{\gamma}_{nl}\mathcal{D}_k h^{mn}\left(\tilde{\gamma}^{ik}\mathcal{D}_m h^{jl} + \tilde{\gamma}^{jk}\mathcal{D}_m h^{il}\right) + \frac{1}{2}\tilde{\gamma}^{ik}\tilde{\gamma}^{kl}\mathcal{D}_l h^{mn}\mathcal{D}_k\tilde{\gamma}_{mn}\Bigg], \tag{1.91}$$

and $\mathcal{D}^2 = \mathcal{D}^i\mathcal{D}_i$ is the Laplacian operator associated with the flat metric with $\mathcal{D}^i \coloneqq f^{ij}\mathcal{D}_j$. The curvature scalar $\tilde{R}$ of the conformal metric does not contain any second order derivative of $\tilde{\gamma}_{ij}$ thanks to the gauge condition

$$\tilde{R} = \frac{1}{4}\tilde{\gamma}^{kl}\mathcal{D}_k h^{ij}\mathcal{D}_l\tilde{\gamma}_{ij} - \frac{1}{2}\tilde{\gamma}^{kl}\mathcal{D}_k h^{ij}\mathcal{D}_j\tilde{\gamma}_{il}. \tag{1.92}$$

Note that the generalized gauge condition result in transverse-traceless (TT) gauge asymtotically, which are well adapted to the treatment of gravitational radiation.

1.5 Constrained scheme for the Einstein equations

Although the ADM equations (eqs. (1.42) to (1.45)) formulate the Einstein equations into a well-defined initial-value problem based on spacetime foliation, it is known to be

unsuitable for numerical simulation of singular spacetime due to the unbounded growth of numerical error (same for conformal decomposition formulation). Several reformulations were developped to maintain stable evolutions. Most of schemes such as BSSN [5, 62], CCZ4 [11], Z4c [10] schemes are based on free-evolution approach where the hyperbolic-type dynamical equations are evolved without enforcing the constraints. The constraint equations are solved only to obtain the initial data and serve as an indicator for numerical errors during the simulation. On the other hand, the fully constrained approach minimizes the hyperbolic-type evolution equations by solving the constraint equations at each time step. Though the elliptic nature of the constraint equations makes it computationally costy to solve, elliptic equations are more stable than hyperbolic equations, and the constraint-violating modes appeared in the free-evolution scheme vanish by construction in fully constrained evolution.

With the efficient elliptic multigrid solvers developped, our relativistic hydrodynamics code `Gmunu` employs the Isenberg–Wilson–Mathews (also known as conformal flatness condition) approximation to the general relativity and the fully constrained formulation. In this section, we introduce the formulations and implementations under the constrained scheme.

1.5.1 Isenberg–Wilson–Mathews approximation

The Isenberg–Wilson–Mathews approximation (IWM), also known as conformal flatness condition (CFC), is a (gravitational-)waveless approximation to general relativity which was independently developped by Isenberg in 1978 [39] as well as Wilson and Mathews in 1989 [80]. In IWM, the spatial metric is approxiated to be conformally flat (hence the name conformal flatness condition)

$$\gamma_{ij} = \psi^4 f_{ij}, \qquad \text{or equivalently} \qquad \tilde{\gamma}_{ij} = f_{ij}, \tag{1.93}$$

under maximal slicing condition $K = 0 = \partial_t K$ (eq. (1.76)) (i.e. $\partial_t \tilde{\gamma}_{ij} = 0$ and $\tilde{D}_i = \mathcal{D}_i$ by construction). The equations for the conformal factor and extrinsic curvature can be obtained from equations (1.56) and (1.57) respectively

$$\partial_t \psi = \beta^i \mathcal{D}_i \psi + \frac{\psi}{6} \mathcal{D}_i \beta^i \tag{1.94}$$

$$K_{ij} = \frac{\psi^4}{2\alpha} \left(f_{jk} \mathcal{D}_i \beta^k + f_{ik} \mathcal{D}_j \beta^k - \frac{2}{3} f_{ij} \mathcal{D}_k \beta^k \right). \tag{1.95}$$

The CFC approximation reduces the ADM equations in a set of coupled non-linear elliptic equations for ψ (from eq. (1.63)), α (from eq. (1.78)), and β^i (from eq. (1.64))

$$\mathcal{D}^2\psi = -\left(2\pi E + \frac{1}{8}K_{ij}K^{ij}\right)\psi^5, \tag{1.96}$$

$$\mathcal{D}^2\left(\alpha\psi\right) = \alpha\psi^5\left[\frac{7}{8}K_{ij}K^{ij} + 2\pi\left(E + 2S\right)\right], \tag{1.97}$$

$$\Delta_L\beta^i = 16\pi\alpha\psi^4 S^i + 2\psi^{10}K^{ij}\mathcal{D}_j\left(\alpha\psi^{-6}\right), \tag{1.98}$$

where $\Delta_L\beta^i \coloneqq \mathcal{D}^2\beta^i + \frac{1}{3}\mathcal{D}^i\mathcal{D}_j\beta^j$ is the *vector Laplacian* (eq. (1.73)) associated with the flat metric f_{ij}. Although the solutions (ψ, α, β^i) to the CFC system do not satisfy all the conformal 3+1 equations in general, it is exact for spherically symmetric spacetime [24] and correct at the 1-PN order in the post-Newtonian expansion of general relativity. The CFC scheme has been successful in numerical simulation for various astrophysical simulation [7–9, 29, 30, 48, 50, 60] and obtained good approximation to full general relativity in axisymmetric rotating neutron stars [21, 29, 30, 63] and in rotating iron core collapses [51].

Extended CFC scheme

Despite the success of CFC scheme in astrophysical simulation, it suffers from the non-uniqueness issue as we discussed in section 1.3.2. A solution to this has been found [26, 60, 64], which involves an extra elliptic equation of the vector potential from CTT decomposition (see section 1.3.3). The resultant scheme is called *extended conformal flatness approximation* (XCFC), and the metric can be solved by following

$$\Delta_L X^i = 8\pi f^{ij}\left(S^*\right)_j, \tag{1.99}$$

$$\mathcal{D}^2\psi = -2\pi E^*\psi^{-1} - \frac{1}{8}\psi^{-7}f_{il}f_{jm}\hat{A}^{lm}\hat{A}^{ij}, \tag{1.100}$$

$$\mathcal{D}^2\left(\alpha\psi\right) = \left(\alpha\psi\right)\left[2\pi\left(E^* + 2S^*\right)\psi^{-2} + \frac{7}{8}\psi^{-8}f_{il}f_{jm}\hat{A}^{lm}\hat{A}^{ij}\right], \tag{1.101}$$

$$\Delta_L\beta^i = 16\pi\alpha\psi^{-6}f^{ij}\left(S^*\right)_j + 2\hat{A}^{ij}\mathcal{D}_j\left(\alpha\psi^{-6}\right), \tag{1.102}$$

where the hydrodynamical conserved quantities are defined as

$$E^* \coloneqq \psi^6 E, \qquad S^* \coloneqq \psi^6 S, \qquad \left(S^*\right)_i \coloneqq \psi^6 S_i, \tag{1.103}$$

and the extra vector elliptic equation (1.99) comes from the momentum constraint (eq. (1.74)) by taking CFC approximation and $\hat{A}^{ij}_{TT} \approx 0$ in CTT decomposition (eq. (1.70)),

which gives

$$\hat{A}^{ij} \approx \mathcal{D}^i X^j + \mathcal{D}^j X^i - \frac{2}{3} f^{ij} \mathcal{D}_k X^k \equiv (LX)^{ij} . \tag{1.104}$$

Unlike the coupled system in IWM approximation, the XCFC system is decoupled in a hierarchical way, and hence guarantees local uniqueness. Once the hydrodynamical conserved quantities are known, the metric equations can be solved accordingly as follows

Step 1: Solve equation (1.99) for the vector potential X^i from the conserved variables $(S^*)_i$.

Step 2: Obtain $\hat{A}^{ij}$ from equation (1.104).

Step 3: Solve equation (1.100) for the conformal factor ψ.

Step 4: Work out S^* using conformal factor ψ.

Step 5: Solve equation (1.101) for the lapse function α.

Step 6: Solve equation (1.102) for the shift vector β^i.

1.5.2 The Meudon-Valencia Fully Constrained Formulation

The fully constrained formulation (FCF) was first proposed by the Meudon group [12], and then later modified by the Valencia's group [23, 26, 27]. By choosing the maximal slcing condition (section 1.4.1) and the generalized Dirac gauge (section 1.4.2), the conformal 3+1 decomposition can be recasted in a coupled elliptic-hyperbolic system, where all the constraint equations are utilized to minimize the number of hyperbolic equations in the system. Here, we summarize the gauge conditions and algebraic constraint for the scheme

$$K \coloneqq \gamma_{ij} K^{ij} = 0, \qquad \text{(maximal slicing condition)} \tag{1.105}$$

$$\mathcal{D}_j h^{ij} = 0, \qquad \text{(generalized Dirac gauge)} \tag{1.106}$$

$$\det \tilde{\gamma}_{ij} = f, \qquad \text{(conformal decomposition)} \tag{1.107}$$

$$K^{ij} = \psi^{-10} \hat{A}^{ij}, \quad \hat{A}^{ij} = \hat{A}^{ij}_{TT} + (LX)^{ij} . \qquad \text{(conformal decomposition)} \tag{1.108}$$

Note that althought it would be more general to used the *Killing operator* $\tilde{L}$ associated with $\tilde{\gamma}_{ij}$ in equation (1.108), the *Killing operator* L associated with flat metric f_{ij} is used since it is easier to handle technically. Under such gauge conditions, the ADM equations are decomposed into a coupled hyperbolic-elliptic system.

Hyperbolic sector

The Valencia's group performed first-order reduction [27] to the reduced FCF system [12] by introducing axuiliary variable

$$w^{ij}{}_{k} \coloneqq \mathcal{D}_k h^{ij}, \tag{1.109}$$

with the gauge condition

$$w^{ij}{}_{i} = 0. \tag{1.110}$$

Thus, the hyperbolic sector in the FCF is recasted as a first-order system in $\left(h^{ij}, \hat{A}^{ij}, w^{ij}{}_{k}\right)$ as follows

$$\partial_t h^{ij} = 2\alpha\psi^{-6}\hat{A}^{ij} + \beta^k w^{ij}{}_{k} - \tilde{\gamma}^{ik}\mathcal{D}_k\beta^j - \tilde{\gamma}^{kj}\mathcal{D}_k\beta^i + \frac{2}{3}\tilde{\gamma}^{ij}\mathcal{D}_k\beta^k, \tag{1.111}$$

$$\begin{aligned}\partial_t \hat{A}^{ij} =& \mathcal{D}_k\left(\frac{1}{2}\alpha\psi^2\tilde{\gamma}^{kl}w^{ij}{}_{l} + \beta^k\hat{A}^{ij}\right) - \hat{A}^{kj}\mathcal{D}_k\beta^i - \hat{A}^{ik}\mathcal{D}_k\beta^j + \frac{2}{3}\hat{A}^{ij}\mathcal{D}_k\beta^k + 2\alpha\psi^{-6}\tilde{\gamma}^{kl}\hat{A}^{ik}\hat{A}^{jl} \\ & - 8\pi\alpha\psi^6\left(\psi^4 S^{ij} - \frac{1}{3}\tilde{\gamma}^{ij}S\right) + \alpha\psi^2\left(\tilde{R}^{ij}_{*} - \frac{1}{3}\tilde{R}\right) + 8\alpha\left(\tilde{\gamma}^{ik}\tilde{\gamma}^{jl} - \frac{1}{3}\tilde{\gamma}^{ij}\tilde{\gamma}^{kl}\right)\mathcal{D}_k\psi\mathcal{D}_l\psi \\ & + 4\psi\left(\tilde{\gamma}^{ik}\tilde{\gamma}^{jl} + \tilde{\gamma}^{il}\tilde{\gamma}^{jk} - \frac{2}{3}\tilde{\gamma}^{kl}\tilde{\gamma}^{ij}\right)\mathcal{D}_k\psi\mathcal{D}_l\alpha - \left(\tilde{\gamma}^{ik}\tilde{\gamma}^{jl} - \frac{1}{3}\tilde{\gamma}^{ij}\tilde{\gamma}^{kl}\right)\mathcal{D}_k\mathcal{D}_l\left(\alpha\psi^2\right) \\ & - \frac{1}{2}\left(\tilde{\gamma}^{ik}w^{lj}{}_{k} + \tilde{\gamma}^{lk}w^{il}{}_{k}\right)\mathcal{D}_l\left(\alpha\psi^2\right),\end{aligned} \tag{1.112}$$

$$\partial_t w^{ij}{}_{k} = \mathcal{D}_k\left(2\alpha\psi^{-6}\hat{A}^{ij} + \beta^k w^{ij}{}_{k} - \tilde{\gamma}^{ik}\mathcal{D}_k\beta^j - \tilde{\gamma}^{kj}\mathcal{D}_k\beta^i + \frac{2}{3}\tilde{\gamma}^{ij}\mathcal{D}_k\beta^k\right), \tag{1.113}$$

where $\tilde{R}^{ij}_{*}$ and $\tilde{R}$ defined in section 1.4.2. This evolution system is proved to be strongly hyperbolic [27] under following conditions

$$\alpha \neq 0, \qquad \alpha^2 - \beta^i\beta_i > 0, \tag{1.114}$$

and the characteristic speed is given by

$$\lambda^i_{\pm} = -\beta^i \pm \alpha\psi^{-2}\tilde{\gamma}^{ii}. \tag{1.115}$$

In Meudon-Valencia's approach, only the transverse-traceless (TT) part of the hyperbolic equations are evolved. Each tensorial hyperbolic equation is reduced to two scalar equations

under TT decomposition [12] and solved using spectral method, and partially implicit Runge-Kutta methods (PIRK) is used to update $w^{ij}{}_k$ to maintain numerical stability [22, 23]. To fulfill the constraint in equation (1.107), the trace part of h^{ij} was calculated by the following iteration procedure:

Step 1: Calculate $h \coloneqq \det \tilde{\gamma}^{ij} - f$.

Step 2: Solve the Poisson equation

$$\mathcal{D}^2\Phi = h. \tag{1.116}$$

Step 3: Update h^{ij} by $h^{ij}_{(new)} = h^{ij}_{(old)} + \frac{1}{2}\left(hf^{ij} - \mathcal{D}^i\mathcal{D}^j\Phi\right)$.

Step 4: Repeat step 1 to 3 until the $\det \tilde{\gamma}^{ij} = f$ is satisfied.

Elliptic sector

The elliptic sector in the FCF scheme is given by

$$\tilde{\gamma}^{kl}\mathcal{D}_k\mathcal{D}_l X^i + \frac{1}{3}\tilde{\gamma}^{ik}\mathcal{D}_k\mathcal{D}_l X^l + \Delta^i{}_{kl}\left(LX\right)^{kl} = 8\pi\tilde{\gamma}^{ij}\left(S^*\right)_j - \Delta^i{}_{kl}\hat{A}^{kl}_{TT}, \tag{1.117}$$

$$\tilde{\gamma}^{kl}\mathcal{D}_k\mathcal{D}_l\psi = -2\pi E^*\psi^{-1} - \frac{1}{8}\psi^{-7}\tilde{\gamma}_{il}\tilde{\gamma}_{jm}\hat{A}^{lm}\hat{A}^{ij} + \frac{1}{8}\psi\tilde{R}, \tag{1.118}$$

$$\tilde{\gamma}^{kl}\mathcal{D}_k\mathcal{D}_l\left(\alpha\psi\right) = \left(\alpha\psi\right)\left[2\pi\psi^{-2}\left(E^* + 2S^*\right) + \frac{7}{8}\psi^{-8}\tilde{\gamma}_{il}\tilde{\gamma}_{jm}\hat{A}^{lm}\hat{A}^{ij} + \frac{\tilde{R}}{8}\right], \tag{1.119}$$

$$\tilde{\gamma}^{kl}\mathcal{D}_k\mathcal{D}_l\beta^i + \frac{1}{3}\tilde{\gamma}^{ik}\mathcal{D}_k\mathcal{D}_l\beta^l = 16\pi\alpha\psi^{-6}\tilde{\gamma}^{ij}\left(S^*\right)_j + 2\hat{A}^{ij}\mathcal{D}_j\left(\alpha\psi^{-6}\right) - 2\alpha\psi^{-6}\Delta^i{}_{kl}\hat{A}^{kl}, \tag{1.120}$$

which can be solved following the same routine as XCFC scheme (section 1.5.1). Note that the FCF scheme is a natural generalization of XCFC scheme since it reduces to XCFC if the approximation $h^{ij} = \hat{A}^{ij}_{TT} = 0$ is made.

passive FCF

The elliptic sector in FCF scheme is technically more difficult to solve. Therefore, the Valencia's group an approximation scheme based on FCF, called passive FCF [23], which neglected the backreaction of the GWs onto the dynamics of the system. Unlike the XCFC which sets the gravitational radiation to zero, the gravitational wave can be evolved in

passive FCF scheme by keeping the hyperbolic sector in FCF scheme, while solving the elliptic sector in XCFC scheme.

1.5.3 The fully-constrained scheme in `Gmunu`

In `Gmunu`, the fully-constrained scheme is solved in a slightly different approach. Instead of solving eqs. (1.111) to (1.113), we omit the axuiliary variable $w^{ij}{}_k$ in order to avoid solving the gauge condition of $w^{ij}{}_k$ 1.110 and evolve the following hyperbolic equations for (h^{ij}, A^{ij})

$$\partial_t h^{ij} = 2\alpha\psi^{-6}\hat{A}^{ij} + \beta^k\mathcal{D}_k h^{ij} - \tilde{\gamma}^{ik}\mathcal{D}_k\beta^j - \tilde{\gamma}^{kj}\mathcal{D}_k\beta^i + \frac{2}{3}\tilde{\gamma}^{ij}\mathcal{D}_k\beta^k, \tag{1.121}$$

$$\begin{aligned}\partial_t \hat{A}^{ij} =& \frac{1}{2}\alpha\psi^2\tilde{\gamma}^{kl}\mathcal{D}_k\mathcal{D}_l h^{ij} + \beta^k\mathcal{D}_k\hat{A}^{ij} - \hat{A}^{kj}\mathcal{D}_k\beta^i - \hat{A}^{ik}\mathcal{D}_k\beta^j + \frac{5}{3}\hat{A}^{ij}\mathcal{D}_k\beta^k + 2\alpha\psi^{-6}\tilde{\gamma}^{kl}\hat{A}^{ik}\hat{A}^{jl} \\ & - 8\pi\alpha\psi^6\left(\psi^4 S^{ij} - \frac{1}{3}\tilde{\gamma}^{ij}S\right) + \alpha\psi^2\left(\tilde{R}^{ij}_* - \frac{1}{3}\tilde{R}\right) + 8\alpha\left(\tilde{\gamma}^{ik}\tilde{\gamma}^{jl} - \frac{1}{3}\tilde{\gamma}^{ij}\tilde{\gamma}^{kl}\right)\mathcal{D}_k\psi\mathcal{D}_l\psi \\ & + 4\psi\left(\tilde{\gamma}^{ik}\tilde{\gamma}^{jl} + \tilde{\gamma}^{il}\tilde{\gamma}^{jk} - \frac{2}{3}\tilde{\gamma}^{kl}\tilde{\gamma}^{ij}\right)\mathcal{D}_k\psi\mathcal{D}_l\alpha - \left(\tilde{\gamma}^{ik}\tilde{\gamma}^{jl} - \frac{1}{3}\tilde{\gamma}^{ij}\tilde{\gamma}^{kl}\right)\mathcal{D}_k\mathcal{D}_l\left(\alpha\psi^2\right) \\ & - \frac{1}{2}\left(\tilde{\gamma}^{ik}\mathcal{D}_k h^{lj} + \tilde{\gamma}^{lk}\mathcal{D}_k h^{il} - \tilde{\gamma}^{kl}\mathcal{D}_k h^{ij}\right)\mathcal{D}_l\left(\alpha\psi^2\right),\end{aligned} \tag{1.122}$$

directly without performing TT composition. Note that although the hyperbolic system is *unconditionally unstable* if second-order explicit *Runge-Kutta* (RK) method used, it has shown to be numerically stable using fourth-order explicit RK method [22, 61]. In `Gmunu`, the hyperbolic sector in FCF scheme is evolving simulataneously with the hydrodynamical system using fourth-order *strong stability-preserving Runge-Kutta* (ssprk) methods. For spatial derivative, fourth-order upwind finite difference is used for the advection terms [61] (i.e. $\mathcal{D}_k h^{ij}$ in eq. (1.121) and $\mathcal{D}_k\hat{A}^{ij}$ in eq. (1.122)), and fourth-order central finite difference is used for other derivative terms.

After the time integration is done, we need to modify $\left(h^{ij}_{old}, \hat{A}^{ij}_{old}\right)$ so that the gauge conditions can be satisfied. The generalized Dirac gauge condition is then enforced by *elliptic divergence cleaning* method as follows

Step 1: Solve the *vector Laplacian* equation

$$\Delta_L W^i = \mathcal{D}_j h^{ij}_{(old)}. \tag{1.123}$$

Step 2: Update h^{ij} by

$$h^{ij}_{(new)} = h^{ij}_{(old)} - (LW)^{ij} \,. \tag{1.124}$$

This treatment is inspired by the divergence cleaning of magnetic monopole in magnetohydrodynamics [2, 3, 74]. In *Gmunu*, a fourth-order central finite difference scheme is used for $\mathcal{D}_j h^{ij}_{old}$, and a second-order central finite difference scheme is used for $\Delta_L W^i$ and $(LW)^{ij}$. To enforce the algebraic constraint (1.107), we modify the trace part of h^{ij} using the same routine described in section 1.5.2.

For $\hat{A}^{ij}$, it can be modified by the following procedures:

Step 1: Obtain the traceless part of $\hat{A}^{ij}_{(old)}$ by

$$\hat{A}^{ij}_{(1)} = \hat{A}^{ij}_{(old)} - \frac{1}{3} f^{ij} f_{kl} \hat{A}^{kl}_{(old)}. \tag{1.125}$$

Step 2: Calculate the vector potential X^i using momentum constraint

$$\tilde{\gamma}^{kl}\mathcal{D}_k\mathcal{D}_l X^i + \frac{1}{3}\tilde{\gamma}^{ik}\mathcal{D}_k\mathcal{D}_l X^l + \Delta^i{}_{kl}\,(LX)^{kl} = 8\pi\tilde{\gamma}^{ij}\,(S^*)_j - \Delta^i{}_{kl}\hat{A}^{kl}_{(1)} - \mathcal{D}_j\hat{A}^{ij}_{(1)}. \tag{1.126}$$

Note that differing from equation (1.117), $\hat{A}^{ij}_{(1)}$ is used on the right-hand-side instead of $\hat{A}^{ij}_{TT}$. Thus, the vector potential X^i here is an additional longitudinal part for $\hat{A}^{ij}$ to satisfy the momentum constraint.

Step 3: Update $\hat{A}^{ij}$ by

$$\hat{A}^{ij}_{(new)} = \hat{A}^{ij}_{(1)} + (LX)^{ij} \,. \tag{1.127}$$

The remaining unknowns (ψ, α, β^i) can then be solved accordingly by adopting the same procedure in section 1.5.2.

Note that we follow the Meudon-Valencia approach and solve the metric variables in orthonormal basis.

Boundary condition

In `Gmunu`, we impose the following boundary conditions for the metric variables at the outermost boundary ($r = r_{max}$)

$$\left.\frac{\partial\psi}{\partial r}\right|_{r=r_{max}} = \frac{1-\psi}{r}, \qquad \left.\frac{\partial\alpha}{\partial r}\right|_{r=r_{max}} = \frac{1-\alpha}{r}, \tag{1.128}$$

$$\left.\frac{\partial\beta^i}{\partial r}\right|_{r=r_{max}} = -\frac{\beta^i}{r}, \qquad \left.\frac{\partial X^i}{\partial r}\right|_{r=r_{max}} = -\frac{X^i}{r}, \qquad \left.\frac{\partial W^i}{\partial r}\right|_{r=r_{max}} = -\frac{W^i}{r}. \tag{1.129}$$

We assume that asymtotically h^{ij} satisfies the linearized quadrupole wave equation [72]

$$\frac{\partial h^{rr}}{\partial t} + \frac{\partial h^{rr}}{\partial r} + \frac{3h^{rr}}{r} = 0, \tag{1.130}$$

$$\frac{\partial h^{r\theta}}{\partial t} + \frac{\partial h^{r\theta}}{\partial r} + \frac{2h^{r\theta}}{r} = 0, \tag{1.131}$$

$$\frac{\partial h^{r\phi}}{\partial t} + \frac{\partial h^{r\phi}}{\partial r} + \frac{2h^{r\phi}}{r} = 0, \tag{1.132}$$

$$\frac{\partial h^{\theta\theta}}{\partial t} + \frac{\partial h^{\theta\theta}}{\partial r} + \frac{h^{\theta\theta}}{r} = 0, \tag{1.133}$$

$$\frac{\partial h^{\theta\phi}}{\partial t} + \frac{\partial h^{\theta\phi}}{\partial r} + \frac{h^{\theta\phi}}{r} = 0, \tag{1.134}$$

$$\frac{\partial h^{\phi\phi}}{\partial t} + \frac{\partial h^{\phi\phi}}{\partial r} + \frac{h^{\phi\phi}}{r} = 0, \tag{1.135}$$

and similarly for $\hat{A}^{ij}$. This boundary condition can be rewritten as [62]

$$Q(t,r) = \left(1 - \frac{\Delta r}{r}\right)^n Q(t - \Delta t, r - \Delta r), \tag{1.136}$$

for $Q(t,r)$ in the Sommerfield form

$$\frac{\partial Q}{\partial t} + \frac{\partial Q}{\partial r} + \frac{nQ}{r} = 0, \tag{1.137}$$

where Δt is the time step, $\Delta r = \alpha\psi^{-}2\Delta t$ and $Q(t - \Delta t, r - \Delta r)$ is obtained by the second-order interpolation from the nearby mesh points.

Chapter 2

Formulations of the Relativistic Hydrodynamics

2.1 Relativistic Hydrodynamics

In the previous chapter, we explored the formulation of the left hand side of the Einstein equations. In this chapter, we focus on the right hand side of the equations, specifically the 3+1 treatment of perfect fluid in conservative form [4, 57].

2.1.1 Perfect fluid

In this section, we consider relativistic *perfect fluid* (i.e. no viscous effects and heat fluxes). The energy-momentum tensor of perfect fluid is given by

$$T^{\mu\nu} = \rho h u^{\mu} u^{\nu} + p g^{\mu\nu}, \tag{2.1}$$

where ρ is the rest-mass density, u^{μ} is the fluid 4-velocity, $h = 1 + \epsilon + \frac{p}{\rho}$ is the enthalpy, p is the pressure, and ϵ is the specific internal energy.
The *Lorentz factor* W of the fluid with respects to the Eulerian observers is given by the projection of fluid 4-velocity u^{μ} to n^{μ}

$$W := -n_{\mu} u^{\mu} = \alpha u^{t}. \tag{2.2}$$

Thus, the spatial 4-velocity of a fluid measured by Eulerian observers is

$$v^{\mu} \coloneqq \frac{\gamma_{\nu}{}^{\mu} u^{\nu}}{W}, \tag{2.3}$$

or in component form

$$v^t = 0, \qquad v^i = \frac{u^i}{W} + \frac{\beta^i}{\alpha}, \tag{2.4}$$

$$v_t = \beta_i v^i, \qquad v_i = \frac{u_i}{W}. \tag{2.5}$$

As a result, the *Lorentz factor* can also be written as

$$W = \frac{1}{\sqrt{1 - v_i v^i}}. \tag{2.6}$$

The dynamics of fluid are governed by the equations of rest-mass conservation and energy momentum conservation. The system is closed by the equation of state (EOS) of the fluid, which reflects the thermodynamic properties of the fluid at a macroscopic level. Here, we consider two common analytic equation of state as follows:

1. Ideal-gas

$$p = (\Gamma - 1)\rho\epsilon, \tag{2.7}$$

   where Γ is the polytropic index of the gas.

2. Polytropic EOS

$$p = K\rho^{\Gamma}, \tag{2.8}$$

   where Γ again is the polytropic index the gas, and K is a constant of proportionality.

2.1.2 Rest-mass conservation

The general-relativistic conservation of rest-mass is given by

$$\nabla_{\mu} J^{\mu} = 0, \qquad J^{\mu} \coloneqq \rho u^{\mu}, \tag{2.9}$$

where J^μ is the rest-mass current density. Under 3+1 decomposition, the rest-mass conservation can be written as

$$\partial_t \left(\sqrt{\gamma} D\right) + \partial_i \left[\sqrt{\gamma} D \left(\alpha v^i - \beta^i\right)\right] = 0, \tag{2.10}$$

where

$$D \coloneqq \rho \alpha u^t = \rho W, \tag{2.11}$$

is the conserved quantity.

2.1.3 Energy and momentum conservation

Other than the conservation of rest-mass, the energy and momentum conservation of the fluid must also be satisfied

$$\nabla_\nu T^{\mu\nu} = 0. \tag{2.12}$$

Following the 3+1 decomposition of stress-energy tensor introduced in equation (1.31), the fluid quantities in the case of perfect fluid become

$$S^{\mu\nu} = \rho h W^2 v^\mu v^\nu + p\gamma^{\mu\nu}, \tag{2.13}$$

$$S^\mu = \rho h W^2 v^\mu, \tag{2.14}$$

$$E = \rho h W^2 - p. \tag{2.15}$$

The conservation of energy and momentum hence leads to

$$\partial_t \left(\sqrt{\gamma} S_j\right) + \partial_i \left[\sqrt{\gamma} \left(\alpha S^i{}_j - \beta^i S_j\right)\right] = \sqrt{\gamma} \left(\frac{1}{2} \alpha S^{ik} \partial_j \gamma_{ik} + S_i \partial_j \beta^i - E \partial_j \alpha\right), \tag{2.16}$$

$$\partial_t \left(\sqrt{\gamma} E\right) + \partial_i \left[\sqrt{\gamma} \left(\alpha S^i - \beta^i E\right)\right] = \sqrt{\gamma} \left(\alpha K_{ij} S^{ij} - S^i \partial_i \alpha\right). \tag{2.17}$$

Equation (2.17) can also be written as

$$\partial_t \left(\sqrt{\gamma} \tau\right) + \partial_i \left[\sqrt{\gamma} \left(\alpha \left(S^i - D v^i\right) - \beta^i \tau\right)\right] = \sqrt{\gamma} \left(\alpha K_{ij} S^{ij} - S^i \partial_i \alpha\right)., \tag{2.18}$$

to recover the energy density in Newtonian limit. where the conserved quantity τ is defined as

$$\tau \coloneqq E - D. \tag{2.19}$$

2.1.4 Conservative form of hydrodynamics equations

Here, we summarize eqs. (2.10), (2.16) and (2.18) and express in conservative form

$$\partial_t \left(\sqrt{\gamma}\mathbf{Q}\right) + \partial_i \left(\sqrt{\gamma}\mathbf{F}^i\right) = \sqrt{\gamma}\mathbf{S}, \tag{2.20}$$

where the conserved variables $\mathbf{Q}$, flux terms $\mathbf{F}^i$ and source terms $\mathbf{S}$ are

$$\mathbf{Q} = \begin{pmatrix} D \\ S_j \\ \tau \end{pmatrix} = \begin{pmatrix} \rho W \\ \rho h W^2 v_j \\ \rho h W^2 - p - D \end{pmatrix}, \tag{2.21}$$

$$\mathbf{F}^i = \begin{pmatrix} D\left(\alpha v^i - \beta^i\right) \\ S_j\left(\alpha v^i - \beta^i\right) + \alpha \delta^i{}_j p \\ \tau left(\alpha v^i - \beta^i + \alpha p v^i \end{pmatrix}, \tag{2.22}$$

$$\mathbf{S} = \begin{pmatrix} 0 \\ \frac{1}{2}\alpha S^{ik}\partial_j \gamma_{ik} + S_i \partial_j \beta^i - E\partial_j \alpha \\ \alpha K_{ij} S^{ij} - S^i \partial_i \alpha \end{pmatrix}, \tag{2.23}$$

which is commonly known as the "*Valencia formulation*" of the relativistic-hydrodynamics equatons.
The characteristic speeds of such system is given by

$$\lambda_0 = \alpha v^i - \beta^i \qquad \text{(triple eigenvalue)}, \tag{2.24}$$

$$\lambda_\pm = \frac{\alpha}{1 - v^2 c_s^2}\left\{ v^i\left(1 - c_s^2\right) \pm c_s^2 \sqrt{\left(1 - v^2\right)\left[\gamma^i i\left(1 - v^2 c_s^2\right) - v^{i\,2}\left(1 - c_s^2\right)\right]} \right\}, \tag{2.25}$$

where $\lambda_\pm$ measures the propagation speeds of the *acoustic waves* of the system, and λ_0 corresponds to the propagation speed of *matter waves*.

2.1.5 Conserved to Primitive variables conversion

It is not trivial to convert the conserved variables (D, S_i, τ) introduced in section 2.1.4 to primitive variables (ρ, W, v^i, p) in relativistic hydrodynamics. One must solve non-linear equations numerically. In `Gmunu`, we adopted the routine used in [33]. The implementation details are included here:

Step 1: Calculate the rescaled variables and some useful relations which are fixed during the iterations

$$S \coloneqq \sqrt{S_i S^i}, \tag{2.26}$$

$$r \coloneqq \frac{S}{D}, \qquad q \coloneqq \frac{\tau}{D}, \qquad k \coloneqq \frac{S}{\tau + D}. \tag{2.27}$$

Step 2: Determine the bounds of the root

$$z_- \coloneqq \frac{k/2}{\sqrt{1 - k^2/4}}, \qquad z_+ \coloneqq \frac{k}{\sqrt{1 - k^2}}. \tag{2.28}$$

Step 3: In the inverval $[z_-, z_+]$, we solve

$$f(z) = z - \frac{r}{\hat{h}(z)}, \tag{2.29}$$

where

$$\hat{h}(z) = (1 + \hat{\epsilon}(z))\,(1 + \hat{a}(z))\,, \tag{2.30}$$

$$\hat{\epsilon}(z) = \hat{W}(z) q - z r + \frac{z^2}{1 + \hat{W}(z)}, \qquad \hat{a}(z) = \frac{\hat{p}(z)}{\hat{\rho}(z)\,(1 + \hat{\epsilon}(z))}, \tag{2.31}$$

$$\hat{p}(z) = p\,(\hat{\rho}(z), \hat{\epsilon}(z))\,, \qquad \hat{\rho}(z) = \frac{D}{\hat{W}(z)}, \qquad \hat{W}(z) = \sqrt{1 + z^2}. \tag{2.32}$$

Equation (2.29) is solved using Illinois algorithm in `Gmunu`. Note that during the iterations, we enforce the density ρ and the specific energy ϵ fail into the validity region of the EOS, i.e., we evalue the updated ρ and ϵ with $\hat{\rho}(z) = \max\left(\min\left(\rho_{\max,\hat{\rho}}\right), \rho_{\min}\right)$ and $\hat{\epsilon}(z) = \max\left(\min\left(\epsilon_{\max,\hat{\epsilon}}\right), \epsilon_{\min}\right)$.

Step 4: With the root z_0 of eq. (2.29), we can then work out the primitive variables (ρ, ϵ, p) respectively with the equations used in step 3. For the velocity v^i, it can be obtained with z by

$$\hat{v}^i(z) = \frac{S^i/D}{\hat{h}(z)\hat{W}(z)}. \tag{2.33}$$

2.2 The reference-metric formalism

The reference-metric formalism, a generalization of the "*Valencia*" formulation, was original proposed by Montero [47] in 2014 for general relativistic hydrodynamics (GRHD) and later extended to ideal magnetohydrodynamics. With the conformal decomposition introduced in section 1.3.1, the determinant of the spatial metric can be rewritten as

$$\begin{aligned} \sqrt{\gamma} &= \psi^6\sqrt{\tilde{\gamma}} \\ &= \sqrt{\hat{\gamma}}\psi^6\sqrt{\tilde{\gamma}/\hat{\gamma}}, \end{aligned} \tag{2.34}$$

where $\hat{\gamma}_{ij}$ is the *time-independent reference metric* which can be chosen to fit the mesh grid in curvilinear coordinate. Therefore, the "*Valencia*" formulation in equation (2.24) can be generalized as

$$\partial_t \mathbf{q} + \hat{\nabla}_i \mathbf{f}^i = \mathbf{s}, \tag{2.35}$$

where $\hat{\nabla}_i$ is the corvariant derivatives sociated with the time-independent reference metric $\hat{\gamma}_{ij}$, $(\mathbf{q}, \mathbf{f}^i, \mathbf{s})$ are the *conformally rescaled* conserved variables, fluxes and source terms respectively.

Comparing to the "*Valencia*" formulation, the hydrodynamical equations in reference-metric approach are numerically more accurate in curvilinear coordinates in multi-dimensional simulation, especially when symmetry is imposed. Equation (2.34) can be further written as

$$\partial_t \mathbf{q} + \frac{1}{\sqrt{\hat{\gamma}}}\partial_j\left(\sqrt{\hat{\gamma}}\mathbf{f}^j\right) = \mathbf{s} + \mathbf{s}_{geom}, \tag{2.36}$$

where $\mathbf{s}_{geom}$ are the *geometrical* source terms which contain the 3-Christoffel symbols $\hat{\Gamma}^i{}_{jk}$ associated with the reference metric $\hat{\gamma}_{ij}$.

Note that the momentum conservation in this expression satisfy to *machine precision* rather than to the level of truncation error due to the fact that the geometrical source terms

$\mathbf{s}_{geom}$ are identically vanishing for the components associated with ignorable coordinates in the metric.

2.2.1 General relativistic hydrodynamics (GRHD) equations

The equations of relativistic hydrodynamics in reference-metric approach is given by

$$\partial_t \left(q_D\right) + \frac{1}{\sqrt{\hat{\gamma}}}\partial_j \left[\sqrt{\hat{\gamma}} \left(f_D\right)^j\right] = 0, \tag{2.37}$$

$$\partial_t \left(q_{S_i}\right) + \frac{1}{\sqrt{\hat{\gamma}}}\partial_j \left[\sqrt{\hat{\gamma}} \left(f_{S_i}\right)^j\right] = s_{S_i} + \hat{\Gamma}^l{}_{ik} \left(f_{S_l}\right)^k, \tag{2.38}$$

$$\partial_t \left(q_\tau\right) + \frac{1}{\sqrt{\hat{\gamma}}}\partial_j \left[\sqrt{\hat{\gamma}} \left(f_\tau\right)^j\right] = s_\tau, \tag{2.39}$$

$$\tag{2.40}$$

The conformally rescaled conserved quantities $\mathbf{q}$ are

$$q_D \coloneqq \psi^6 \sqrt{\tilde{\gamma}/\hat{\gamma}} D = \psi^6 \sqrt{\tilde{\gamma}/\hat{\gamma}} \left(\rho W\right), \tag{2.41}$$

$$q_{S_i} \coloneqq \psi^6 \sqrt{\tilde{\gamma}/\hat{\gamma}} S_i = \psi^6 \sqrt{\tilde{\gamma}/\hat{\gamma}} \left(\rho h W^2 v_i\right), \tag{2.42}$$

$$q_\tau \coloneqq \psi^6 \sqrt{\tilde{\gamma}/\hat{\gamma}} \tau = \psi^6 \sqrt{\tilde{\gamma}/\hat{\gamma}} \left(\rho h W^2 - p - D\right). \tag{2.43}$$

The flux terms $\mathbf{f}^i$ are

$$\left(f_D\right)^i \coloneqq \psi^6 \sqrt{\tilde{\gamma}/\hat{\gamma}} \left(D \hat{v}^i\right), \tag{2.44}$$

$$\left(f_{S_j}\right)^i \coloneqq \psi^6 \sqrt{\tilde{\gamma}/\hat{\gamma}} \left(S_j \hat{v}^i + \delta^i{}_j \alpha p\right), \tag{2.45}$$

$$\left(f_\tau\right)^i \coloneqq \psi^6 \sqrt{\tilde{\gamma}/\hat{\gamma}} \left(\tau \hat{v}^i + \alpha p v^i\right), \tag{2.46}$$

where $\hat{v}^i \coloneqq \alpha v^i - \beta^i$.
Finally, the source terms $\mathbf{s}$ are

$$s_D = 0, \tag{2.47}$$

$$s_{S_i} = \alpha \psi^6 \sqrt{\tilde{\gamma}/\hat{\gamma}} \left[-T^{00} \alpha \partial_i \alpha + T^0{}_k \hat{\nabla}_i \beta^k + \frac{1}{2} \left(T^{00} \beta^j \beta^k + 2 T^{0j} \beta^k + T^{jk}\right) \hat{\nabla}_i \gamma_{jk}\right], \tag{2.48}$$

$$s_\tau = \alpha \psi^6 \sqrt{\tilde{\gamma}/\hat{\gamma}} \left[T^{00} \left(K_{ij} \beta^i \beta^j - \beta^k \partial_k \alpha\right) + 2 T^{0j} \left(2 K_{jk} \beta^k - \partial_j \alpha\right) + T^{ij} K_{ij}\right]. \tag{2.49}$$

Part II

Methodology: Numerical methods and tests

Chapter 3

Numerical Methods

In this chapter, we are going to discuss the details of the numerical method used in `Gmunu` [18, 19]. In the fully-constrained scheme, the evolution of relativistic hydrodynamics in dynamical spacetime consists of a set of coupled hyperbolic-elliptic system. Firstly, we discuss the numerical method adopted for the hyperbolic system in `Gmunu`, including the high-resolution shock-capturing (HRSC) method and the finite volume method. Then, we discuss the multigrid solver in `Gmunu`, which is used to solve the elliptic system.

3.1 High-resolution shock-capturing (HRSC) methods

The high-resolution shock-capturing (HRSC) methods is a class of methods commonly used to reproduce accurately the discontinuous features in the solution with no spurious oscillation [35]. Note that the HRSC methods can be distinguished in *finite-difference (conservative)* method which evolves the *pointwise values* of the solution, and *finit-volume (conservative)* method which evolves the *cell average* of the solution. Although the accuracy of finite-difference method can be extended to higher order easily, it is extremely diffcult to extend the method to general non-uniform grids [45]. On the other hand, the finite-volume methods are natural to conservative scheme as well as non-structured grid, but the multidimensional reconstruction algorithm is complicated and computational expensive especially for higher-order method.

In this section, we will first discuss the finite-volume conservative methods, and then focus on the *Godunov methods* which guarantee the upwind property of conservative non-linear equations [43].

3.1.1 Finite-volume conservative methods

Given the conservative equation in orthogonal coordinate system (x^1, x^2, x^3) in form

$$\partial_t \mathbf{q} + \frac{1}{\sqrt{\hat{\gamma}}} \hat{\nabla}_i \left(\sqrt{\hat{\gamma}} \mathbf{f}^i \right) = \mathbf{s} + \mathbf{s}_{geom}, \tag{3.1}$$

where $\mathbf{q}$ are the conserved variables, $\mathbf{f}^i$ are the flux terms, $\mathbf{s}$ are the source terms and $\mathbf{s}_{geom}$ are the geometrical source term which is related to the 3-Christoffel symbol $\hat{\Gamma}^i{}_{jk}$ of the reference metric $\hat{\gamma}_{ij}$. We can then discretize equation (3.1) on a computational domain divided into $N_1 \times N_2 \times N_3$ cells. Each cells can be represented by a tuple of integers (i, j, k) where $1 \leq i \leq N_1$, $1 \leq j \leq N_2$ and $1 \leq k \leq N_3$. The cell bounds are given by

$$(x^1_{i-1/2}, x^1_{i+1/2}), \qquad (x^2_{j-1/2}, x^2_{j+1/2}), \qquad (x^3_{k-1/2}, x^3_{k+1/2}). \tag{3.2}$$

Thus, the mesh cell spacings are

$$\Delta x^1_i = x^1_{i+1/2} - x^1_{i-1/2}, \qquad \Delta x^2_j = x^2_{j+1/2} - x^2_{j-1/2}, \qquad \Delta x^3_k = x^3_{k+1/2} - x^3_{k-1/2}, \tag{3.3}$$

and the cell centres are

$$x^1_i = \frac{1}{2}\left(x^1_{i+1/2} + x^1_{i-1/2}\right), \quad x^2_j = \frac{1}{2}\left(x^2_{j+1/2} - x^2_{j-1/2}\right), \quad x^3_k = \frac{1}{2}\left(x^3_{k+1/2} - x^3_{k-1/2}\right). \tag{3.4}$$

By integrating equation 3.1 over cell volume and applying divergence theorem on the flux terms, it becomes

$$\begin{aligned} \frac{d}{dt}\langle \mathbf{q} \rangle_{i,j,k} = -\frac{1}{\Delta V_{i,j,k}} \Bigg\{ & \left[\left(\langle \mathbf{f} \rangle^1 \Delta A^1 \right)\Big|_{i+1/2,j,k} - \left(\langle \mathbf{f} \rangle^1 \Delta A^1 \right)\Big|_{i-1/2,j,k} \right] \\ & + \left[\left(\langle \mathbf{f} \rangle^2 \Delta A^2 \right)\Big|_{i,j+1/2,k} - \left(\langle \mathbf{f} \rangle^2 \Delta A^2 \right)\Big|_{i,j-1/2,k} \right] \\ & + \left[\left(\langle \mathbf{f} \rangle^3 \Delta A^3 \right)\Big|_{i,j,k+1/2} - \left(\langle \mathbf{f} \rangle^3 \Delta A^3 \right)\Big|_{i,j,k-1/2} \right] \Bigg\} \\ & + \langle \mathbf{s} \rangle_{i,j,k} + \langle \mathbf{s}_{geom} \rangle_{i,j,k} \end{aligned} \tag{3.5}$$

where the cell volume and the volume-average are defined as

$$\Delta V_{i,j,k} \coloneqq \int_{cell} \sqrt{\hat{\gamma}} dx^1 dx^2 dx^3, \qquad \langle \bullet \rangle \coloneqq \frac{1}{\Delta V_{i,j,k}} \int_{cell} \bullet \sqrt{\hat{\gamma}} dx^1 dx^2 dx^3 \tag{3.6}$$

, while the cell surface and the surface-average are defined as

$$\Delta A^i \coloneqq \int_{surface} \sqrt{\hat{\gamma}} dx^{j,j\neq i}, \qquad \langle \bullet \rangle \coloneqq \frac{1}{\Delta A^i} \int_{surface} \bullet \sqrt{\hat{\gamma}} dx^{j,j\neq i}. \tag{3.7}$$

Since the reference metric $\hat{\gamma}_{ij}$ is time-independent, the cell volume, cell surface and the volume-averaged 3-Christoffel symbols $\left\langle \hat{\Gamma}^i{}_{jk} \right\rangle$ in the geometrical source term are determined once the coordinate is chosen. We have included these quantities in Appendix.

3.1.2 Godunov methods

For simplicity, we consider one-dimensional hyperbolic conservation laws

$$\partial_t \mathbf{q}(x,t) + \partial_x \mathbf{f}[\mathbf{q}(x,t)] = 0, \tag{3.8}$$

We apply the discretization on spatial domain into computing cell I_j with size Δx

$$I_j = \left[x_{j-1/2}, x_{j+1/2}\right], \qquad \Delta x = x_{j+1/2} - x_{j-1/2}, \tag{3.9}$$

and time slices $[t^n, t^{n+1}]$. Thus, equation (3.8) can be recasted into a *conservative* scheme as

$$\langle \mathbf{q} \rangle_j^{n+1} = \langle \mathbf{q} \rangle_j^n + \frac{\Delta t}{\Delta x} \left(\langle \mathbf{f} \rangle_{j-1/2} - \langle \mathbf{f} \rangle_{j+1/2} \right), \tag{3.10}$$

where

$$\langle \mathbf{q} \rangle_j^n \coloneqq \frac{1}{\Delta x} \int_{x_{j-1/2}}^{x_{j+1/2}} \mathbf{q}(x, t^n)\, dx \tag{3.11}$$

is the *cell-average* and

$$\langle \mathbf{f} \rangle_{j\pm1/2} \coloneqq \frac{1}{\Delta t} \int_{t^n}^{t^{n+1}} \mathbf{f}\left[\mathbf{q}\left(x_{j\pm1/2}, t\right)\right] dt \tag{3.12}$$

is the *numerical fluxes*.

In Godunov's original approach [42], he considered a piecewise-constant distribution of

data

$$\mathbf{q}(x,t^n) = \begin{cases} \langle \mathbf{q} \rangle_j^n & \text{if } x \leq x_{j+1/2}, \\ \langle \mathbf{q} \rangle_{j+1}^n & \text{if } x > x_{j+1/2}, \end{cases} \tag{3.13}$$

and built a local Riemann problem $\mathcal{RP}\left(\langle \mathbf{q} \rangle_L, \langle \mathbf{q} \rangle_R\right)$ with left state $\langle \mathbf{q} \rangle_L = \langle \mathbf{q} \rangle_j^n$ and right state $\langle \mathbf{q} \rangle_R = \langle \mathbf{q} \rangle_{j+1}^n$. Therefore, the numerical fluxes

$$\langle \mathbf{f} \rangle_{j+1/2} = \frac{1}{\Delta t} \int_{t^n}^{t^{n+1}} \mathbf{f}\left[\mathbf{q}\left(x_{j+1/2}, t\right)\right] dt = \mathcal{F}\left(\langle \mathbf{q} \rangle_j^n, \langle \mathbf{q} \rangle_{j+1}^n\right) \tag{3.14}$$

only depends on the two constant states $\langle \mathbf{q} \rangle_j^n$ and $\langle \mathbf{q} \rangle_{j+1}^n$.
Note that the Godunov method is a *monotone method*. Consider an explicit method of the type

$$\langle \mathbf{q} \rangle_j^{n+1} = \mathcal{H}\left(\langle \mathbf{q} \rangle_j^n, \langle \mathbf{q} \rangle_{j\pm1}^n, \langle \mathbf{q} \rangle_{j\pm2}^n, \ldots, \langle \mathbf{q} \rangle_j^{n-m}, \langle \mathbf{q} \rangle_{j\pm1}^{n-m}, \langle \mathbf{q} \rangle_{j\pm2}^{n-m}, \ldots\right). \tag{3.15}$$

The method is *monotone* if

$$\frac{\partial \mathcal{H}}{\partial \langle \mathbf{q} \rangle_j^n} \geq 0 \quad \forall \langle \mathbf{q} \rangle_j^n. \tag{3.16}$$

From this definition, we can further prove that given the data $\{\langle \mathbf{q} \rangle_j^n\}$, the solution $\{\langle \mathbf{q} \rangle_j^{n+1}\}$ obtained by a monotone method is

$$\max_j\{\langle \mathbf{q} \rangle_j^{n+1}\} \leq \max_j\{\langle \mathbf{q} \rangle_j^n\}, \qquad \min_j\{\langle \mathbf{q} \rangle_j^{n+1}\} \geq \min_j\{\langle \mathbf{q} \rangle_j^n\}, \tag{3.17}$$

that is, no spurious new extrema introduced in the solution as time evolves.

3.1.3 Reconstruction scheme

The Godunov method introduced in the previous section is only first-order accurate in space and time because of the piecewise-constant distribution of data. In practice, the spatial accuracy can be higher than first-order if the left state $\langle \mathbf{q} \rangle_L$ and right state $\langle \mathbf{q} \rangle_R$ of the Riemann problem at the cell interface $x_{j+1/2}$ are *reconstructed* using a higher-order polynomial representation of $\mathbf{q}$ rather than $\langle \mathbf{q} \rangle_j^n$ and $\langle \mathbf{q} \rangle_{j+1}^n$.
One of the reconstruction techniques are the *slope-limiter* methods which improve the piecewise-constant representation by providing a piecewise-linear reconstruction of $\mathbf{q}^n(x)$

at each cell

$$\mathbf{q}_j^n(x) = \langle \mathbf{q} \rangle_j^n + \sigma_j^n \left(x - x_j \right) \qquad \text{for } x_{j-1/2} \leq x \leq x_{j+1/2}, \tag{3.18}$$

where σ_j^n is the slope of the linear reconstruction. Here, we list out several common slope-limiters

Minmod slope-limiter The *minmod slope-limiter* [41, 79, 88] is given by

$$\sigma_j^n \coloneqq \text{minmod} \left(\frac{\langle \mathbf{q} \rangle_j^n - \langle \mathbf{q} \rangle_{j-1}^n}{\Delta x}, \frac{\langle \mathbf{q} \rangle_{j+1}^n - \langle \mathbf{q} \rangle_j^n}{\Delta x} \right), \tag{3.19}$$

where

$$\text{minmod}\left(\alpha, \beta\right) \coloneqq \begin{cases} \alpha & \text{if } |\alpha| < |\beta| \text{ and } \alpha\beta > 0, \\ \beta & \text{if } |\alpha| > |\beta| \text{ and } \alpha\beta > 0, \\ 0 & \text{if } \alpha\beta \leq 0, \end{cases} \tag{3.20}$$

$$\coloneqq \frac{1}{2} \left[\text{sgn}\alpha + \text{sgn}\beta \right] \min\left(|\alpha|, |\beta| \right). \tag{3.21}$$

Monotonized central-difference (MC) limiter The MC limiter [77] is given by

$$\sigma_j^n \coloneqq \text{minmod} \left(\frac{\langle \mathbf{q} \rangle_{j+1}^n - \langle \mathbf{q} \rangle_{j-1}^n}{2\Delta x}, \frac{\langle \mathbf{q} \rangle_j^n - \langle \mathbf{q} \rangle_{j-1}^n}{\Delta x}, \frac{\langle \mathbf{q} \rangle_{j+1}^n - \langle \mathbf{q} \rangle_j^n}{\Delta x} \right), \tag{3.22}$$

where

$$\text{minmod}\left(\alpha, \beta, \gamma\right) \coloneqq \begin{cases} \min\left(\alpha, \beta, \gamma\right) & \text{if } \alpha, \beta, \gamma > 0, \\ \max\left(\alpha, \beta, \gamma\right) & \text{if } \alpha, \beta, \gamma < 0, \\ 0 & \text{otherwise.} \end{cases} \tag{3.23}$$

Note that the methods mentioned above are *total variation diminishing (TVD)*. The total variation of a solution at time t^n is defined as

$$\text{TV}\left(\langle \mathbf{q} \rangle^n \right) \coloneqq \sum_i \left| \langle \mathbf{q} \rangle_{j+1}^n - \langle \mathbf{q} \rangle_j^n \right|, \tag{3.24}$$

which measures the oscillations appeared in the solution. A numerical method is called *total variation diminishing (TVD)* if it satisfies

$$\mathrm{TV}\left(\langle \mathbf{q} \rangle^{n+1}\right) \leq \mathrm{TV}\left(\langle \mathbf{q} \rangle^{n}\right), \quad \forall \langle \mathbf{q} \rangle^{n}, \tag{3.25}$$

which shows that the oscillations of the solution in TVD method are reduced.
Here, we list out all the possible reconstruction schemes in `Gmunu` in Table 3.1.

Table 3.1 Reconstruction schemes available in `Gmunu`.

Order of accuracy	2nd	3rd	5th	7th
	Minmod [41, 79, 88]	PPM [20]	MP5 [70]	WENO7
	MC [77]	Koren	WENO5	MP-WENO7
	Superbee [58]	Cada3	WENO5-Z	EXENO7
	Vanleer [78]	WENO3	WENO5-Z+	
	Albada	WENO3-YC-3	WENO-NM-5	
	MC-beta		WENO-NM-Z	
	Cada		WENO-NM-Z+	
	Venk			

3.1.4 Approximate Riemann solver

As discussed in section 3.4.2, the Godunov method requires the solution of local *Riemann problem* $RP\left(\langle \mathbf{q} \rangle_L, \langle \mathbf{q} \rangle_R\right)$ at the cell interface $x_{j+1/2}$ involving the left state $\langle \mathbf{q} \rangle_L$ and right state $\langle \mathbf{q} \rangle_R$. Although the exact solution of the Riemann problem is available in relativistic hydrodynamics, it is computational costy in multidimensional case. Therefore, an *approximate Riemann solver* is used in `Gmunu` which is computationally less expensive and yet very accurate in general. Approximation Riemann solver can be divided into two types

(i) *Complete Riemann solver* which contains all the charateristic fields of the exact solution, and

(ii) *Incomplete Riemann solver* which only contains a subset of them.

In this section, we discuss some commonly used incomplete Riemann solver in `Gmunu`. For a comprehensive introduction, we refer readers to [75].

The HLL solver This Riemann solver was proposed by Harten, Lax and van Leer [36], hence the name *HLL Riemann solver*. The solution is approximated by

$$\mathbf{q}(x,t) = \begin{cases} \mathbf{q}_L & \text{if } x/t < \lambda_L, \\ \mathbf{q}_{HLL} & \text{if } \lambda_L \leq x/t \leq \lambda_R, \\ \mathbf{q}_R & \text{if } x/t > \lambda_R, \end{cases} \tag{3.26}$$

where $\lambda_L \leq 0$ and $\lambda_R \geq 0$ are the minimum and maximum of the characteristic speeds respectively

$$\lambda_L \coloneqq \min\left(0, \lambda_-\left(\mathbf{q}_L\right), \lambda_-\left(\mathbf{q}_R\right)\right), \tag{3.27}$$

$$\lambda_L \coloneqq \max\left(0, \lambda_+\left(\mathbf{q}_L\right), \lambda_+\left(\mathbf{q}_R\right)\right), \tag{3.28}$$

and $\lambda_\pm$ are given by the eigenvalues of the hydrodynamics equations. The single constant state $\mathbf{q}_{HLL}$ is given by

$$\mathbf{q}_{HLL} = \frac{\lambda_R \mathbf{q}_R - \lambda_L \mathbf{q}_L + \mathbf{f}_L - \mathbf{f}_R}{\lambda_R - \lambda_L}. \tag{3.29}$$

Thus, the numerical fluxes can be calculated as

$$\mathbf{f} = \begin{cases} \mathbf{f}_L & \text{if } x/t < \lambda_L, \\ \mathbf{f}_{HLL} & \text{if } \lambda_L \leq x/t \leq \lambda_R, \\ \mathbf{f}_R & \text{if } x/t > \lambda_R, \end{cases} \tag{3.30}$$

where the HLL fluxes are

$$\mathbf{f}_{HLL} = \frac{\lambda_R \mathbf{f}_L - \lambda_L \mathbf{f}_R + \lambda_L \lambda_R \left(\mathbf{q}_R - \mathbf{q}_L\right)}{\lambda_R - \lambda_L} \tag{3.31}$$

The Rusanov solver The *Rusanov approximate Riemann solver* [59], also known as the *total variation diminishing Lax-Friedrichs (TVDLF) flux* [67], is a special case of the HLL Riemann solver where the condition $\lambda_R = -\lambda_L = \lambda$ is imposed. As a result, the Rusanov flux can be reduced from equation (3.31) as

$$\mathbf{f}_{Rusanov} = \frac{1}{2}\left(\mathbf{f}_L + \mathbf{f}_R\right) - \frac{1}{2}\lambda\left(\mathbf{q}_R - \mathbf{q}_L\right), \tag{3.32}$$

where one can take the single speed λ to be $\lambda = \max\left(|\lambda_L|, |\lambda_R|\right)$.

3.2 Time discretization

3.2.1 Explicit Runge-Kutta method

To perform the time integration, one can expand time derivative using Taylor expansion

$$\partial_t \mathbf{q} = \frac{1}{2\Delta t}\left(\mathbf{q}^{n+1} - \mathbf{q}^{n-1}\right). \tag{3.33}$$

However, it is not a practical time integration scheme because

(i) Large amount of data for the previous time steps is need to be stored in higher-order scheme.

(ii) Stability is not guaranteed.

In constract, in the Runge-Kutta (RK) methods, we do not need to store large amount of data, and it enables stable time integration for higher-order-accurate scheme. Consider a system of equations in form

$$\frac{d\mathbf{q}}{dt} = \mathbf{F}\left(\mathbf{q}, t\right), \tag{3.34}$$

where $\mathbf{F}$ denotes the right-hand side of the equation. The general m-stage explicit Runge-Kutta method of the Shu-Osher form [66] is

$$\mathbf{q}^{(0)} = \mathbf{q}^n \tag{3.35}$$

$$\mathbf{q}^{(i)} = \sum_{k=0}^{i-1}\left[\alpha_{ik}\mathbf{q}^{(k)} + \Delta t\beta_{ik}\mathbf{F}\left(\mathbf{q}^{(k)}, t^n + \gamma_k\Delta t\right)\right], \quad i = 1, 2, \ldots, m \tag{3.36}$$

$$\mathbf{q}^{n+1} = \mathbf{q}^{(m)}, \tag{3.37}$$

where the coefficient α_{ik}, β_{ik} and γ_k are chosen such that the order conditions are satisfied.

Strong stability-preserving (explicit) Runge-Kutta methods

The strong stability-preserving Runge-Kutta (SSPRK) methods [65, 66] is special class of RK methods which maintains total variation diminishing property (3.25) in higher-order time integration scheme. Due to its non-oscillatory property, the SSPRK methods are desirable in problems with discontinuities and strong shocks [37].
As mentioned in section 1.5.3, the hyperbolic system in the FCF scheme becomes unconditionally unstable if first-order or second-order explicit RK method is used. As a

result, we use fourth-order SSPRK scheme to evolve the FCF hyperbolic sector and the hydrodynamics equation in `Gmunu`.

3.2.2 Courant-Friedrichs-Lewy conditions

One necessary condition for stability is the *Courant-Friedrichs-Lewy* (CFL) conditions [28]. From a physical point of view, the CFL condition ensures that the propagation speed of any physical perturbation is always smaller than the numerical speed $_N$

$$|\lambda| \leq \lambda_N \coloneqq \frac{\Delta x}{\Delta t}. \tag{3.38}$$

Therefore, the time steps for the time integration can be obtained by

$$\Delta t = c_{CFL} \min_k \left(\frac{\Delta x}{|\lambda_k|} \right), \tag{3.39}$$

where $c_{CFL} \leq 1$ is a dimensionless constant and λ_k is the charateristic speed of the evolution system.

3.3 Atmosphere treatment

One of the challenge in astrophysical simulation is handle the interface between fluid and vacuum where the density ρ, pressurece p and velocities v^i vanish. In this section, we outline the positivity preserving limiter [19, 38] used in `Gmunu` for atmosphere handling.

3.3.1 Positivity preserving limiter

We consider a discretized first-order Euler timestep

$$\frac{u_i^{n+1} - u_i^n}{\Delta t} = \frac{1}{\delta V_i} \left(f_{i-1/2} \Delta A_{i-1/2} - f_{i+1/2} \Delta A_{i+1/2} \right), \tag{3.40}$$

$$\Rightarrow u_i^{n+1} = \frac{1}{2} \left(u_i^+ - u_i^- \right), \tag{3.41}$$

where

$$u_i^- \coloneqq \left(u_i^n - 2\frac{\Delta t}{\Delta V_i} f_{i+1/2} \Delta A_{i+1/2} \right), \tag{3.42}$$

$$u_i^+ \coloneqq \left(u_i^n + 2\frac{\Delta t}{\Delta V_i} f_{i-1/2} \Delta A_{i-1/2} \right), \tag{3.43}$$

To ensure the positivity of u_i^+ and u_i^-, we modify the flux as [38]

$$f_{i+1/2} = \theta f_{i+1/2}^{HO} + (1-\theta) f_{i+1/2}^{LO}, \tag{3.44}$$

where $f_{i+1/2}^{HO}$ is the original high-order flux scheme and $f_{i+1/2}^{LO}$ is the first order Lax-Friedrichs flux. The parameter $\theta \in [0,1]$ is the maximum value such that u_i^+ and u_i^- are positive. Since the Lax-Friedrichs scheme is positivity preserving, we can always choose θ to preserve the positvity. Note that once the positivity in one first-order Euler timestep is preserved, the positivity is guaranteed for any strong-stability preserving Runge-Kutta (SSPRK) time integrator.

In `Gmunu`, we implemented the positivity preserving limiter in conserved density D and energy density τ to preserve the positivity of density ρ and pressure p. For the multidimensional case, we apply the limiter with component-by-component approach.

3.4 Multigrid Method for elliptic equations

3.4.1 Overview

The elliptic equations can be solved using *iterative methods* such as Jocabi method, Gauss-Seidel (GS) method and successive overrelaxation (SOR) [86]. These methods are very effective in eliminating high-frequency or oscillatory components of the error, but less effective in reducing low-frequency or smooth components of the error since the changes of error are only made with spatially locally correction [16]. This problem will become even more severe for higher resolution because the convergence rate behaves like $1 - \mathcal{O}(h^2)$. Since the smooth modes in a fine grid become oscillatory in a coarser grid, one can move to a coarser grid to smooth out the low-frequency mode error and return back to the fine grids. This is the key idea of the multigrid method.

In the multigrid method, the key ingredients are

(i) **Multigrid cycle scheme** tells the structure of the multigrid solver (see Figure 3.1 for example).

(ii) **Restriction** maps the values from the fine grid to the coarse grid.

(iii) **Prolongation** maps the values from the coarse grid to the fine grid.

(iv) **Smoother** to smooth out the error at different levels.

(v) **Direct solver** to solve the equation at the coarsest level.

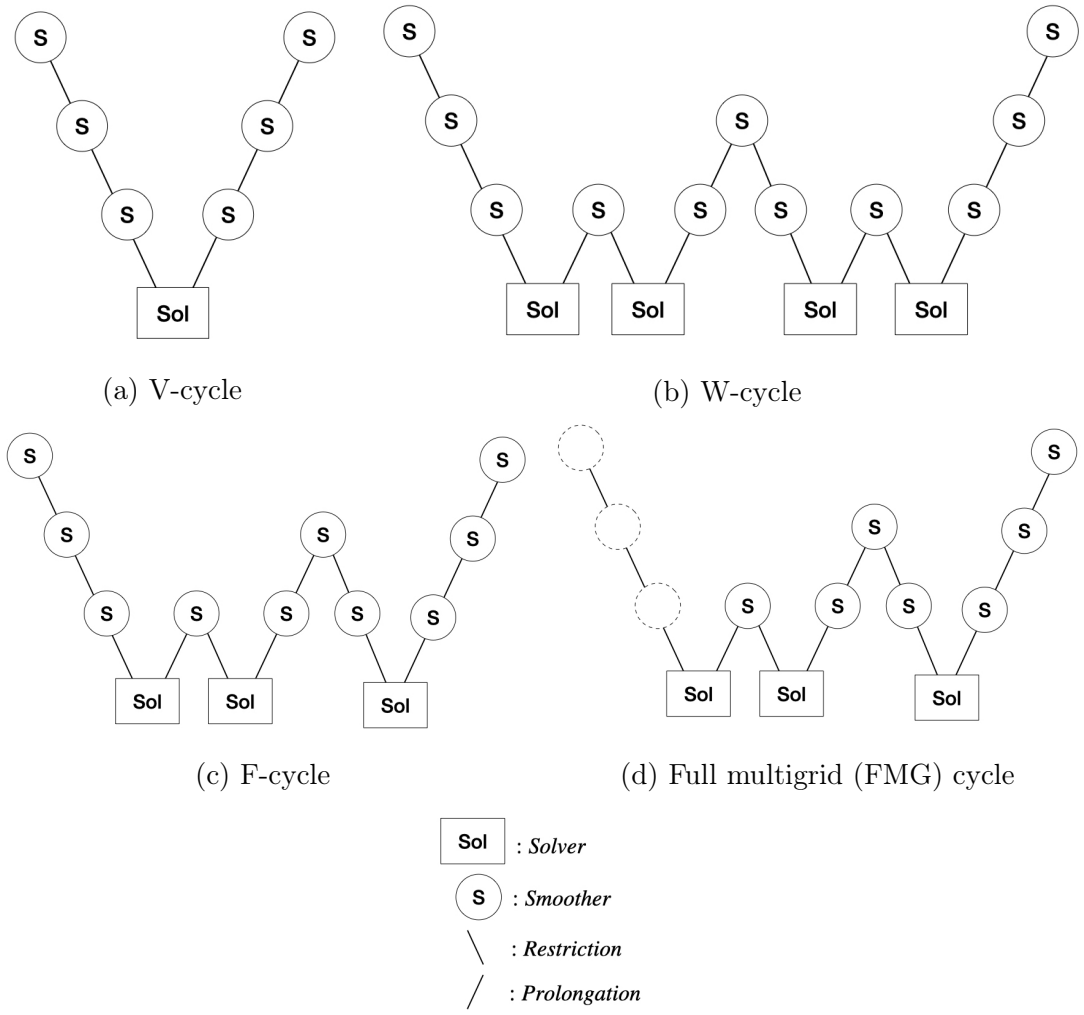

Fig. 3.1 "S" denotes smoothing. "Sol" denotes direct solver. Descending line \ denotes restriction and ascending line / denotes prolongation.

For more comprehensive discussion of multigrid method, we refer the readers to [15, 16, 76, 86].

3.4.2 Cell-centred discretization and operator

Given a non-linear elliptic equation

$$\mathcal{L}(u) = f, \tag{3.45}$$

with elliptic operator $\mathcal{L}$, solution u and source term f, it can be discretized as

$$\mathcal{L}_h(u_h) = f_h, \tag{3.46}$$

where $\mathcal{L}_h$ is the discretized operator with resolution h, u_h and f_h are solution and source term defined at the cell-centres.

Laplacian operator

The Laplacian operator is one of the elliptic operators that commonly used in `Gmunu`, including the constraint eqs. (1.100) and (1.101) in XCFC scheme and the algebraic constraint eq. (1.116) in the FCF scheme. It is discretized with a standard 5/7-point (in 2D/3D) second-order accurate discretization. The details of the discretization in different geometry is shown in Appendix A.

Mixed derivatives

In the elliptic sector of the FCF scheme (eqs. (1.117) to (1.120)) and the vector elliptic equations in the XCFC scheme (eqs. (1.99) and (1.102)), the elliptic operators contain mixed derivative terms $\frac{\partial^2 u}{\partial x \partial y}$. We use second-order accuracy discretization as follows

$$\left(\frac{\partial^2 u}{\partial x \partial y}\right)_{i,j,k} = \frac{u_{i+1,j+1,k} - u_{i-1,j+1,k} - u_{i+1,j-1,k} + u_{i-1,j-1,k}}{4\Delta x \Delta y} \tag{3.47}$$

Convection-diffusion equation

In the momentum constraint (eqs. (1.117) and (1.126)) of the FCF scheme, the elliptic operator contains a convective term $\Delta^i{}_{kl}\,(LX)^{kl}$ which has a similar form as the following

$$\frac{\partial^2 u}{\partial x^2} + a\frac{\partial u}{\partial x} = 0. \tag{3.48}$$

While the Laplacian operator in equation (3.48) is discretized using standard 5/7-point approximation, the convection term needs to be discretized using upwind method [76]. In

`Gmunu`, we adopts second-order accuracy lopsided spatial finite differencing as

$$\left(\frac{\partial u}{\partial x}\right)_i = \frac{1}{2\Delta x}\begin{cases} 3u_i - 4u_{i-1} + u_{i-2} & a \leq 0, \\ -3u_i + 4u_{i+1} - u_{i+2} & a \geq 0. \end{cases} \tag{3.49}$$

3.4.3 Smoothers and solvers

Another essential element in multigrid method is the smoothers and direct solvers. In `Gmunu`, we implemented the point-wise *Newton Gauss-Seidel* smoothers [55]

$$u^{new}_{i,j,k} = u^{old}_{i,j,k} - \left(\mathcal{L}\left(u^{old}_{i,j,k}\right) - f_{i,j,k}\right) \Big/ \left(\frac{\partial \mathcal{L}}{\partial u_{i,j,k}}\Big|_{u=u^{old}_{i,j,k}}\right), \tag{3.50}$$

where the components of the new approximation are used as soon as they are computed. Note that if *mathcalL* is linear in u, the Newton Gauss-Seidel method reduces to the standard Gauss-Seidel method.
There are two order of sweeping through the components $u_{i,j,k}$ implemented in `Gmunu`.

1. *Standard Gauss-Seidel* which follows the linear order of the indexes i, j, k, stored in computer's memory.

2. *Red-black Gauss-Seidel* which sweeps through all the even indexes first (i.e. $i+j+k$ is even) then the odd indexes.

Although the convergence rate of the smoothers is lowered in 2D/3D spherical and 3D cylindrical coordinate due to the anisotropy [76], currently we still implemented the smoothers for all coordinate. For simplicity, we adopt the Newton Gauss-Seidel method for the direct solver.

3.4.4 Transfer operators: restriction and prolongation

The transfer operators connect data at different level. The *restriction* operators map the values from the fine grid to the coarse grid, while the *prolongation* operators map the values from the coarse grid to the fine grid. For prolongation, we use linear interpolation based on the nearest neighbors [73, 74, 87], which can be described by the following:

$$u_{x+h/2,y+h/2} = \frac{1}{4}\left(2u_{x,y} + u_{x+h,y} + u_{x,y+h}\right) + \mathcal{O}\left(h^2\right), \tag{3.51}$$

$$u_{x-h/2,y+h/2} = \frac{1}{4}\left(2u_{x,y} + u_{x-h,y} + u_{x,y+h}\right) + \mathcal{O}\left(h^2\right), \tag{3.52}$$

or in stencil notation

$$\frac{1}{4}\left[\begin{array}{ccccc} \cdot & 1 & & 1 & \cdot \\ 1 & 2 & & 2 & 1 \\ & & * & & \\ 1 & 2 & & 2 & 1 \\ \cdot & 1 & & 1 & \cdot \end{array}\right]^{h}_{2h},$$

where the "$*$" denotes the location of the coarse grid and the notation shows the weighting of the value which are the neighbours of the coarse grid node "$*$". For restriction, the value of four (2D) or eight (3D) fine grid values is averaged to obtain a coarse grid value.

3.4.5 The Full Approximation Scheme

To solve the non-linear elliptic equations, we adopt the Full Approximation Scheme (FAS) [13, 14, 18, 55, 74]. Here, we briefly outline the FAS algorithm. we define the residual r

$$r \coloneqq f - \mathcal{L}(v), \tag{3.53}$$

where f is the right-hand side of the equation, $\mathcal{L}$ is the elliptic operator and v is an approximation solution. For the discretized equation with resolution h, we have

$$r_h = f_h - \mathcal{L}_h(v_h). \tag{3.54}$$

The current approximation v_h is then restricted to coarse grid $v_{2h} = \mathcal{R}(v_h)$ where $\mathcal{R}$ is the restriction operator. A copy of $v_{2h}^{old} = v_{2h}$ is stored for later usage. The coarse-grid right-hand side is then update as

$$f_{2h} = \mathcal{R}(r_h) + \mathcal{L}_{2h}(v_{2h}). \tag{3.55}$$

Smoothing steps are then applied to the coarse grid. In the prolongation steps, the solution is updated with a correction from the coarse grid as

$$v_h = v_h + \mathcal{P}\left(v_{2h} - v_{2h}^{old}\right), \tag{3.56}$$

where $mathcalP$ is the prolongation operator. In practise, this procedure will be repeated until the solution converges (i.e. the L_∞ norm of the residual is below chosen threshold value).

Since the current version of `Gmunu` is built upon the framework of `AMRVAC 2.0` [40, 81], it is natural use the open-source geometric multigrid library `octree-mg` [74] which is MPI-parallelized, support quadtree/octree AMR grids, and provide periodic, Dirichlet, and Neumann boundary conditions. Nonetheless, the library only supports 2D/3D Cartesian coordinate and 2D cylindrical coordinate. We extended it to support multidimensional spherical and cylindrical coordinates as well as the Robin boundary condition. In addition, only a single layer of ghost cell without diagonal cell is used in `octree-mg`. In order to calculate the mixed derivatives and solve the convection-diffusion problems, we extend the library to support multiple layers of ghost cells with diagonal cells, which also allow us to explore higher-order scheme in the future.

Chapter 4

Numerical Tests and Results

4.1 Multigrid solver tests

4.1.1 Newtonian gravitational field

For simplicity, we consider only the test of Poisson equation. In Newtonian gravity, the gravitational potential Φ can be obtained by

$$\nabla^2\Phi = -4\pi\rho, \tag{4.1}$$

where ρ is the energy density of the matter source. Here, we consider a spherically symmetric source as

$$\rho(r) = \begin{cases} \rho_0\left(1-r^2\right), & r<1, \\ 0, & r\geq 1, \end{cases} \tag{4.2}$$

where ρ_0 is a constant chosen to be 1. The analytic solution is given by

$$\Phi(r) = \begin{cases} \pi\rho_0\left(\frac{r^4}{5}-\frac{2r^2}{3}+1\right), & r<1, \\ \frac{8\pi\rho_0}{15r}, & r\geq 1. \end{cases} \tag{4.3}$$

We solve the Poisson equation (4.1) in 1D spherical, 2D cylindrical and 3D Cartesian coodinates with 2nd order and 4th order central finite difference respectively. The computational domain and the discretization are set to be $0\leq r\leq 10$ and $[N]$ for spherical coordinate, $0\leq(r,z)\leq 10$ and $[N,N]$ for cylindrical coordinate, and $0\leq(x,y,z)\leq 10$ and $[N,N,N]$ for Cartesian coordinate respectively, where N is the number of grids. The

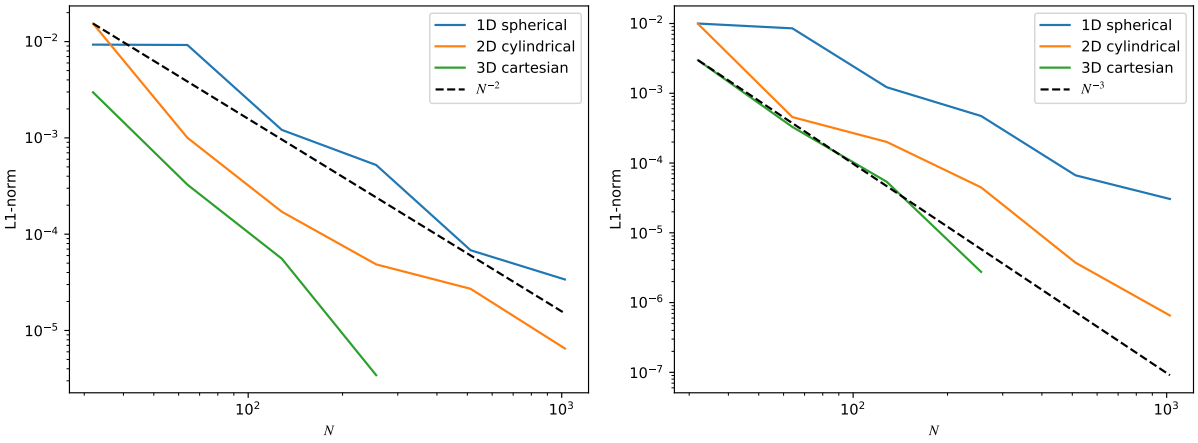

Fig. 4.1 L1-norm of Φ using 2nd order (left) and 4th order central finite difference scheme (right).

boundary conditions are set to be

$$\left.\frac{d\Phi}{dr}\right|_{r=0} = 0 \qquad \text{(Neumann boundary condition)}, \tag{4.4}$$

$$\left.\frac{dr\Phi}{dr}\right|_{r=10} = 0 \qquad \text{(Robin boundary condition.)} \tag{4.5}$$

Note that although the boundition condition should be $\Phi \to 0$ for $r \to \infty$, in practice we can only impose the Robin boundary condition for large r due to the finite computational domain.

Figure 4.1 shows the convergent rate of the L1-norm of Φ

$$||\Phi\ ||_1 = \frac{1}{N}\sum_{i=1}^{N}\left|\Phi_i - \Phi_i^{exact}\right|, \tag{4.6}$$

where arround second-order accuracy and third-order convergence is achieved for 2nd order and 4th order central finite difference scheme in general.

4.2 Teukolsky wave test

We consider the quadrupole $(l, m) = (2, 0)$ mode of the vacuum solution. For even-parity quadrupole mode, the metric takes form [72] in spherical coordinate (r, θ, ϕ)

$$\begin{aligned} ds^2 =& -dt^2 + (1 + Af_{rr})\, dr^2 + (2Bf_{r\theta})\, r dr d\theta + (2Bf_{r\phi})\, r \sin\theta dr d\phi \\ & \left(1 + Cf^{(1)}_{\theta\theta} + Af^{(2)}_{\theta\theta}\right) r^2 d\theta^2 + \left[2\left(A - 2C\right) f_{\theta\phi}\right] r^2 \sin\theta d\theta d\phi \\ & + \left(1 + Cf^{(1)}_{\phi\phi} + Af^{(2)}_{\phi\phi}\right) r^2 \sin^2\theta d\phi^2, \end{aligned} \tag{4.7}$$

where the coefficient A, B, C are constructed from $F(x)$ for $x = t - r$ outgoing wave and $x = t + r$ ingoing wave

$$F(x) = F_1(t - r) + F_2(t + r), \tag{4.8}$$

and we define

$$F^{(n)} := \left.\frac{d^n F_1(x)}{dx^n}\right|_{x=t-r} + (-1)^n \left.\frac{d^n F_2(x)}{dx^n}\right|_{x=t+r}. \tag{4.9}$$

Thus, the coefficient are given by

$$A = 3\left(\frac{F^{(2)}}{r^3} + \frac{3F^{(1)}}{r^4} + \frac{3F}{r^5}\right), \tag{4.10}$$

$$B = -\left(\frac{F^{(3)}}{r^2} + \frac{3F^{(2)}}{r^3} + \frac{3F^{(1)}}{r^4} + \frac{6F}{r^5}\right), \tag{4.11}$$

$$C = \frac{1}{4}\left(\frac{F^{(4)}}{r} + \frac{2F^{(3)}}{r^2} + \frac{9F^{(2)}}{r^3} + \frac{21F^{(1)}}{r^4} + \frac{21F}{r^5}\right). \tag{4.12}$$

For $m = 0$ mode, the angular function f_{ij} are given by

$$f_{rr} = 2 - 3\sin^2\theta, \qquad f_{r\theta} = -3\sin\theta\cos\theta, \qquad f_{r\phi} = 0, \tag{4.13}$$

$$f^{(1)}_{\theta\theta} = 3\sin^2\theta, \qquad f^{(2)}_{\theta\theta} = -1, \qquad f_{\theta\phi} = 0, \tag{4.14}$$

$$f^{(1)}_{\phi\phi} = -f^{(1)}_{\theta\theta}, \qquad f^{(2)}_{\phi\phi} = 3\sin^2\theta - 1. \tag{4.15}$$

In our test, we consider

$$F_1(x) = -F_2(x) = \frac{\mathcal{A}}{2} x e^{-\frac{x^2}{\lambda^2}}, \tag{4.16}$$

and perform the simulation in 2D axisymmetric cylindrical coordinate (r, z, ϕ) with z reflection symmetry. The computational domain covers the region $0 \leq \rho \leq 5$, $0 \leq z \leq 5$ and the discretization of the domain is set to be $[256, 256]$. The inital profile is given by

$$\psi = \alpha = 1, \tag{4.17}$$

$$\beta^i = 0, \tag{4.18}$$

$$h^{rr} = \mathcal{A}' \frac{\lambda^4 - \rho^2 z^2}{\lambda^8} e^{-\frac{x^2}{\lambda^2}}, \tag{4.19}$$

$$h^{rz} = \mathcal{A}' \frac{\rho z \left(\rho^2 - 2\lambda^2\right)}{\lambda^8} e^{-\frac{x^2}{\lambda^2}}, \tag{4.20}$$

$$h^{r\phi} = 0, \tag{4.21}$$

$$h^{zz} = -\mathcal{A}' \frac{(2\lambda^4 - 4\lambda^2\rho^2 + \rho^4)}{\lambda^8} e^{-\frac{x^2}{\lambda^2}}, \tag{4.22}$$

$$h^{z\phi} = 0, \tag{4.23}$$

$$h^{\phi\phi} = \mathcal{A}' \frac{(\lambda^4 - 4\lambda^2\rho^2 + \rho^2 z^2 + \rho^4)}{\lambda^8} e^{-\frac{x^2}{\lambda^2}}, \tag{4.24}$$

$$\hat{A}^{ij} = 0, \tag{4.25}$$

where $\mathcal{A}' = \frac{\mathcal{A}}{12}$. The analytic solution is written in the Appendix C. The simulation will be performed under two configurations:

1. Solve the hyperbolic equations only (without elliptic divergence cleaning).
2. Solve the hyperbolic equations togather with the elliptic sector in FCF except ψ, α and β (with elliptic divergence cleaning).

In the tests, we choose $\mathcal{A}' = 10^{-4}$ and $\lambda = 1$. In figure 4.2, it shows the L2-norm of h^{ij} which is given by

$$\delta h^{ij} = \sqrt{\frac{1}{V} \sum \left| h^{ij} - h^{ij}_{exact} \right|^2}. \tag{4.26}$$

The simulation result agrees with the analytical solution very well. In figure 4.3, it shows that the elliptic divergence cleaning method is effective on reducing the divergence of h^{ij}. Especially for $t \gtrsim 5$ when the wave is propagated out of the computational domain, the divergence of h^{ij} keep increasing if no treatment is applied, while it is suppressed with the elliptic cleaning method. In figure 4.4, we show the evolution of the $h^{\phi\phi}$ component with elliptic divergence cleaning.

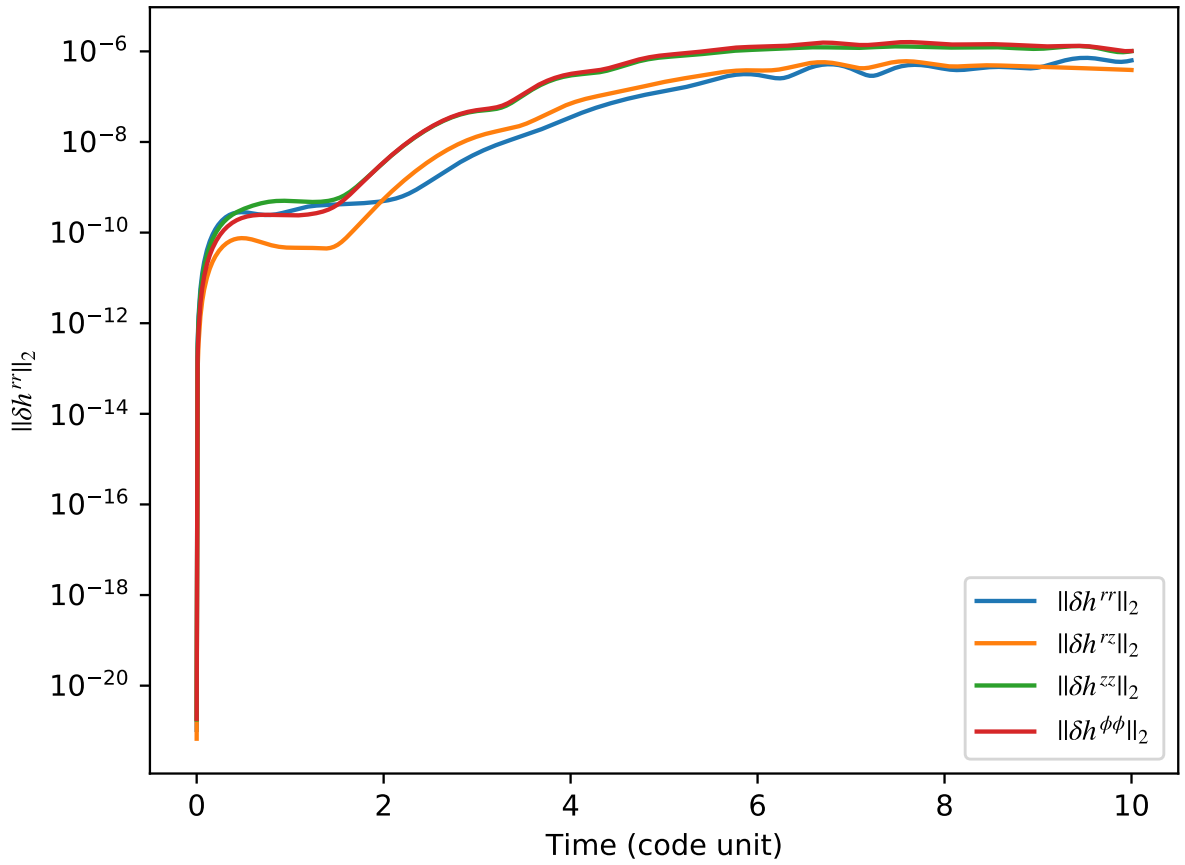

Fig. 4.2 L2-norm of h^{ij} of the Teukolsky wave test by solving hyperbolic equations without elliptic sector (configuration 1).

4.3 General relativistic hydrodynamics in dynamic spacetime

Here we study the evolution of a neutron star with dynamical background under FCF scheme and passive FCF scheme.

4.3.1 Non-rotating neutron star

In this test, we consider a non-rotating neutron star known as "BU0" [30] which is constructed with the polytropic index $\Gamma = 2$ and $K = 100$, and central rest-mass density $\rho_c = 1.28 \times 10^{-3}$ (in $c = G = M_\odot = 1$ unit). This star model is generated by the open-source code `XNS` [17, 52–54]. We simulate the star in 2D cylindrical coordinate and impose z reflection symmetry. The computational domain covers $0 \leq r \leq 60$, $0 \leq z \leq 60$

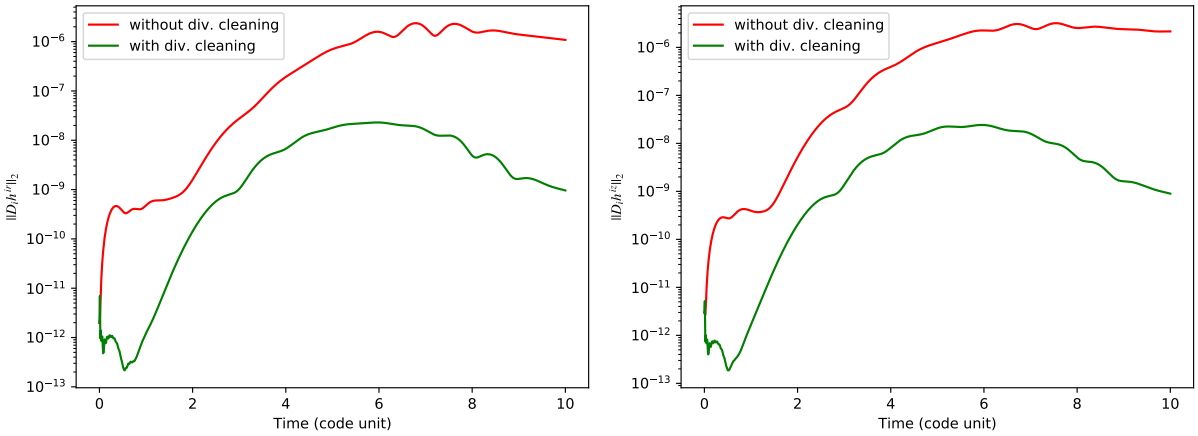

(a) L2-norm of $\mathcal{D}_i h^{ir}$ (b) L2-norm of $\mathcal{D}_i h^{iz}$

Fig. 4.3 L2-norm of the divergence of h^{ij}. The red line corresponds to the evolution of h^{ij} without divergence cleaning while the green line corresponds to the evolution of h^{ij} with divergence cleaning.

in code unit with resolution $n_r \times n_z = 256 \times 256$. The ideal-gas equation of state with $\Gamma = 2$ is used for the simulation. We extract the plus polarization of gravitational wave signal h_+ at $(r_{ext}, z_{ext}) = (40, 0)$ which is given by

$$h_+ \approx \frac{h^{\phi\phi} - h^{zz}}{2} \frac{R_{ext}}{R}, \tag{4.27}$$

where $R = \sqrt{r^2 + z^2}$ is the extraction radius.

Figure 4.5 shows the extracted gravitational wave signal h_+ from "BU0". Note that since the BU0 is a shperically symmetric star and it is simulated without any initial perturbation, only F mode can be extracted which its value agrees with [30].

4.3.2 Rapidly rotating neutron star

In this test, we consider a rapidly-rotating neutron star known as "BU8" [30]. The polytropic index, K value and central rest-mass density are the same as "BU0", except that it is uniformly rotating at an angular velocity of $\Omega = 2.633 \times 10^{-2}$. The simulation setups are same as section 4.3.1, and again we extracted h_+ at $(r_{ext}, z_{ext}) = (40, 0)$.

Figure 4.6 shows the extracted gravitational wave signal h_+ from "BU8". The extracted pulsation mode agrees with [30] for F and ${}^2f$ mode. Note that the initial profile "BU8" is constructed under CFC approximation with zero h^{ij}, which is not the case when full GR is considered. This is why a spurious oscillation in h occurs at the beginning of the

simulation. Nonetheless, h quickly settles down and oscillates around the new equilibrium position. We also observed that the ${}^2f$ mode of h_+ in FCF scheme has a higher amplitude compared to passive FCF scheme.

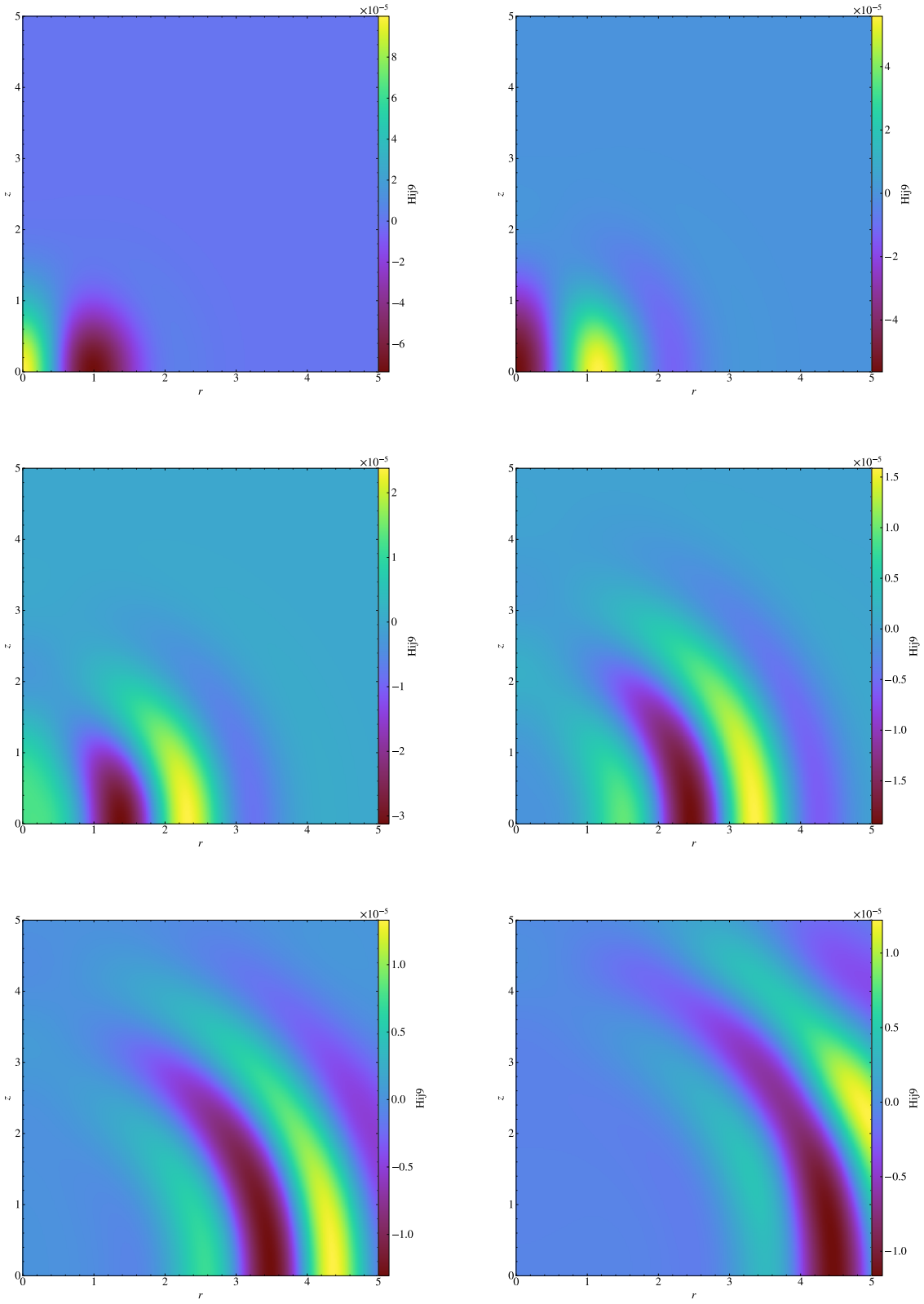

Fig. 4.4 Evolution of $h^{\phi\phi}$ component between $t = 0$ (upper left) and $t = 5$ (lower right) with elliptic divergence cleaning.

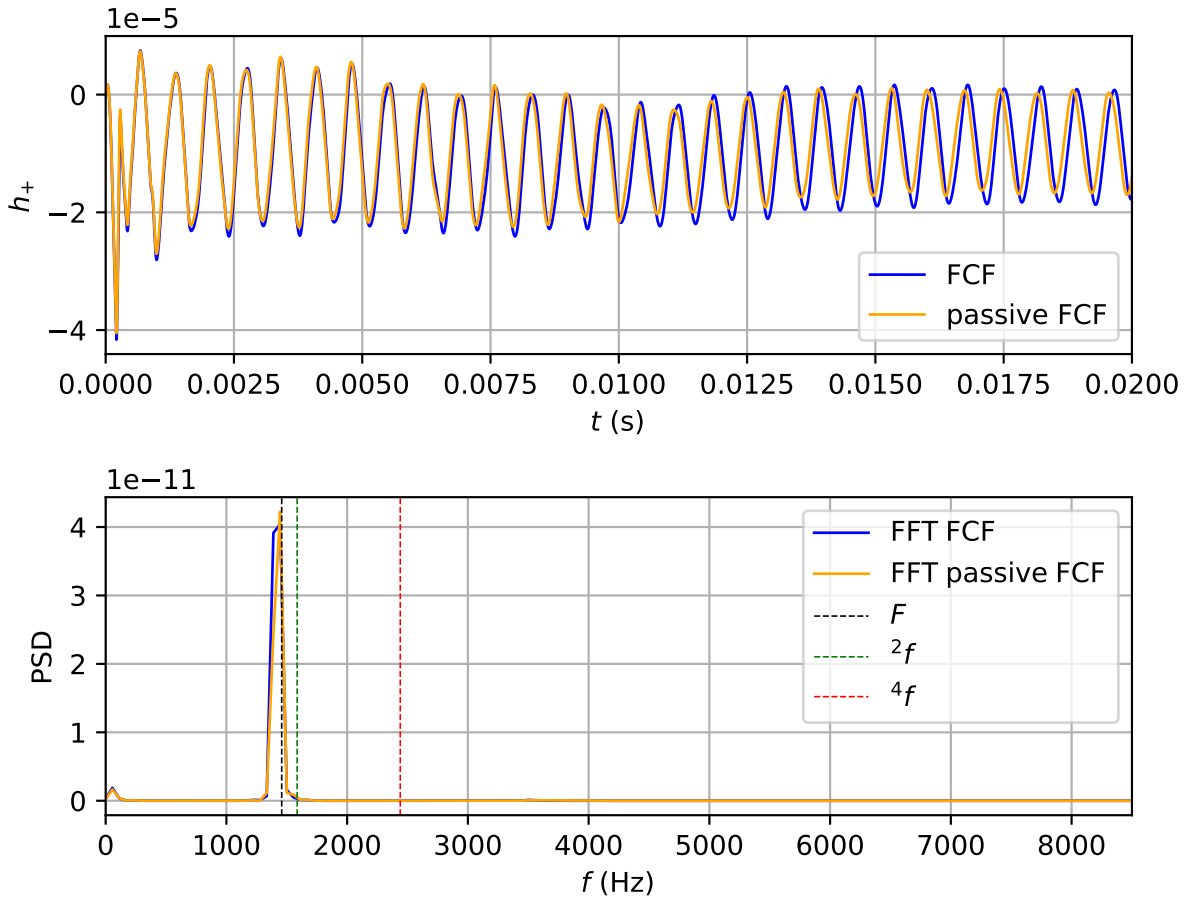

Fig. 4.5 (upper panel) h_+ extracted at $(r_{ext}, z_{ext}) = (40, 0)$ from the simulations of oscillating neutron star "BU0". (lower panel) The power spectral density of h_+. The vertical lines represent the known and well-tested eigenmode frequencies [30]

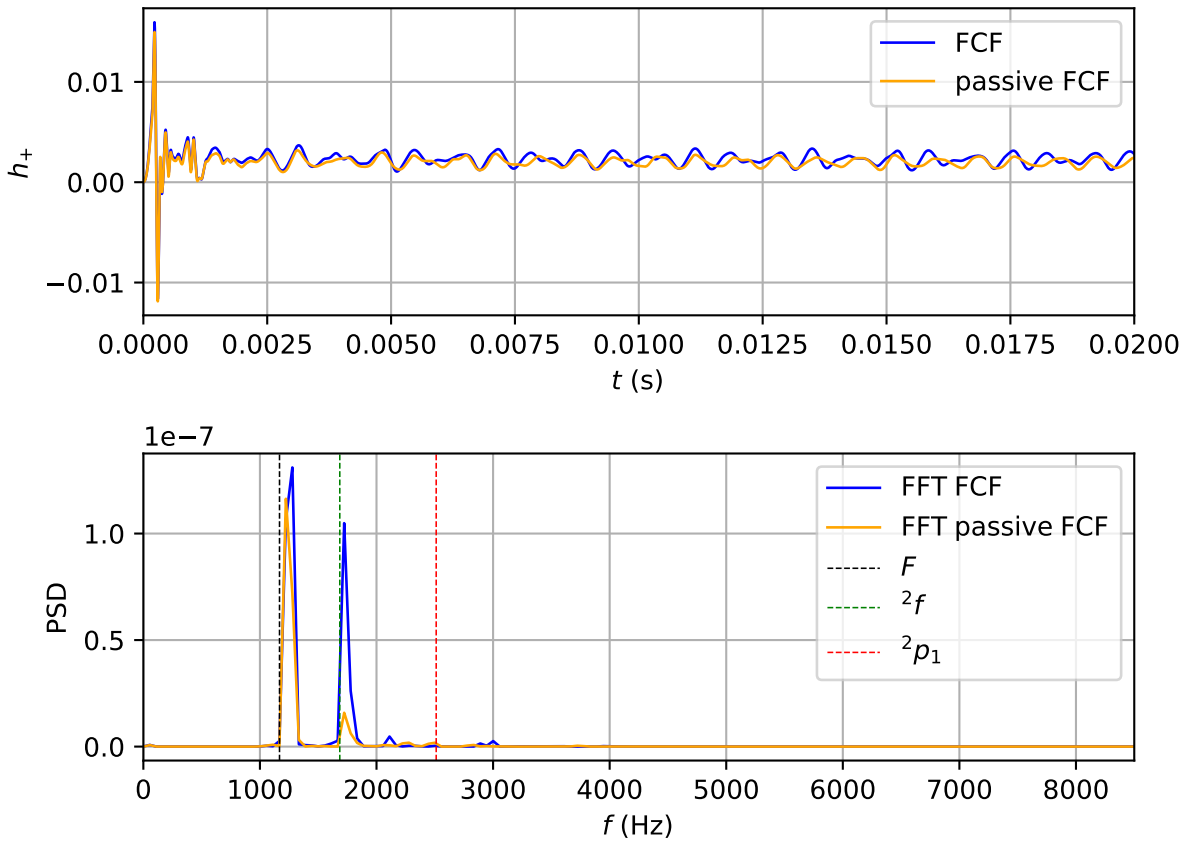

Fig. 4.6 (upper panel) h_+ extracted at $(r_{ext}, z_{ext}) = (40, 0)$ from the simulations of oscillating neutron star "BU8". (lower panel) The power spectral density of h_+ calculated from $t = 2.5ms$ due to the spurios oscillation at the beginning. The vertical lines represent the known and well-tested eigenmode frequencies [30]

Part III

Conclusion

Chapter 5

Concluding Remarks

The main theme of this work is to extend the `Gmunu` code to adopt the fully constrained formulation (FCF) scheme, a full general relativistic formulation naturally generalized from the conformal flatness condition (CFC) approximation which is current used in the code. So far only two-dimensional cylindrical coordinate is implemented for the FCF and passive FCF scheme. In this thesis, we present the methodology and implementation of `Gmunu` in detail.
We have tested `Gmunu` with several benchmarking tests. In the Teukolsky wave test, we have shown the stability and convergence of evolving the hyperbolic equations in FCF. We also demonstrated that the elliptic divergence cleaning using multigrid method is able to maintain the gauge condition. For the hydrodynamics, we have performed simulations of the evolution of both non-rotating and rotating neutron stars. We are able to extract the gravitational wave signature directly from the metric components.

Future Plan

Here, we list some possible improvement of `Gmunu` planned for the future.

Support different geometries Currently, the FCF scheme is only implemented in 2D cylindrical coordinate which limit our study to axisymmetric profiles. We will extend the code to support 2D spherical as well as 3D spherical/Cartesian coordinates in the future so that we can broaden our study to non-axisymmetric systems such as binary systems and supernovae.

Simulate black holes In `Gmunu`, we have no treatment to handle the black holes singularity nor the apparent horizon. It has been shown that the excision scheme can be used to deal with black holes for constrained evolution scheme in spherically symmetric spacetime [25]. Therefore, we would like to develop a horizon finder in `Gmunu` and implement the excision scheme in the future.

Improve the FCF scheme We used finite-difference scheme for solving Einstein equations and conservative finite-volume scheme for solving the hydrodynamics. Although the volume average value and point-wise value are differed by the second-order error, making them equivalent in second-order method, this becomes a problem if we extend the code to high-order numerical methods in the future. It has been suggested that the hyperbolic sector in FCF can be rewritten in conservative form [27]. Therefore, we would like to rewrite the hyperbolic equations in FCF to suit the finite-volume scheme in the future.

References

[1] R Amowitt, S Deser, and CW Misner. "The dynamics of general relativity". In: *Gravitation: An Introduction to Current Research* (1962), pp. 227–265.

[2] Dinshaw S Balsara. "Total variation diminishing scheme for adiabatic and isothermal magnetohydrodynamics". In: *The Astrophysical Journal Supplement Series* 116.1 (1998), p. 133.

[3] Dinshaw S Balsara and Jongsoo Kim. "A comparison between divergence-cleaning and staggered-mesh formulations for numerical magnetohydrodynamics". In: *The Astrophysical Journal* 602.2 (2004), p. 1079.

[4] Francesc Banyuls et al. "Numerical {3+ 1} general relativistic hydrodynamics: A local characteristic approach". In: *The Astrophysical Journal* 476.1 (1997), p. 221.

[5] Thomas W Baumgarte and Stuart L Shapiro. "Numerical integration of Einstein's field equations". In: *Physical Review D* 59.2 (1998), p. 024007.

[6] Thomas W Baumgarte and Stuart L Shapiro. *Numerical relativity: solving Einstein's equations on the computer*. Cambridge University Press, 2010.

[7] A Bauswein, N Stergioulas, and H-T Janka. "Revealing the high-density equation of state through binary neutron star mergers". In: *Physical Review D* 90.2 (2014), p. 023002.

[8] Andreas Bauswein, Stéphane Goriely, and H-T Janka. "Systematics of dynamical mass ejection, nucleosynthesis, and radioactively powered electromagnetic signals from neutron-star mergers". In: *The Astrophysical Journal* 773.1 (2013), p. 78.

[9] Andreas Bauswein et al. "Equation-of-state dependence of the gravitational-wave signal from the ring-down phase of neutron-star mergers". In: *Physical Review D* 86.6 (2012), p. 063001.

[10] Sebastiano Bernuzzi and David Hilditch. "Constraint violation in free evolution schemes: Comparing the BSSNOK formulation with a conformal decomposition of the Z4 formulation". In: *Physical Review D* 81.8 (2010), p. 084003.

[11] Carles Bona et al. "General-covariant evolution formalism for numerical relativity". In: *Physical Review D* 67.10 (2003), p. 104005.

[12] Silvano Bonazzola et al. "Constrained scheme for the Einstein equations based on the Dirac gauge and spherical coordinates". In: *Physical Review D* 70.10 (2004), p. 104007.

[13] Keeran J Brabazon, Matthew E Hubbard, and Peter K Jimack. "Nonlinear multigrid methods for second order differential operators with nonlinear diffusion coefficient". In: *Computers & Mathematics with Applications* 68.12 (2014), pp. 1619–1634.

[14] Achi Brandt. "Multi-level adaptive solutions to boundary-value problems". In: *Mathematics of computation* 31.138 (1977), pp. 333–390.

[15] Achi Brandt and Oren E Livne. *Multigrid Techniques: 1984 Guide with Applications to Fluid Dynamics, Revised Edition*. SIAM, 2011.

[16] William L Briggs, Van Emden Henson, and Steve F McCormick. *A multigrid tutorial*. SIAM, 2000.

[17] N Bucciantini and L Del Zanna. "General relativistic magnetohydrodynamics in axisymmetric dynamical spacetimes: the X-ECHO code". In: *Astronomy & Astrophysics* 528 (2011), A101.

[18] Patrick Chi-Kit Cheong, Lap-Ming Lin, and Tjonnie Guang Feng Li. "Gmunu: toward multigrid based Einstein field equations solver for general-relativistic hydrodynamics simulations". In: *Classical and Quantum Gravity* 37.14 (2020), p. 145015.

[19] Patrick Chi-Kit Cheong et al. "Gmunu: Paralleled, grid-adaptive, general-relativistic magnetohydrodynamics in curvilinear geometries in dynamical spacetimes". In: *arXiv preprint arXiv:2012.07322* (2020).

[20] Phillip Colella and Paul R Woodward. "The piecewise parabolic method (PPM) for gas-dynamical simulations". In: *Journal of computational physics* 54.1 (1984), pp. 174–201.

[21] Gregory B Cook, Stuart L Shapiro, and Saul A Teukolsky. "Testing a simplified version of Einstein's equations for numerical relativity". In: *Physical Review D* 53.10 (1996), p. 5533.

[22] Isabel Cordero-Carrión and Pablo Cerdá-Durán. "Partially implicit Runge-Kutta methods for wave-like equations". In: *arXiv preprint arXiv:1211.5930* (2012).

[23] Isabel Cordero-Carrión, Pablo Cerdá-Durán, and José Marı´a Ibáñez. "Gravitational waves in dynamical spacetimes with matter content in the fully constrained formulation". In: *Physical Review D* 85.4 (2012), p. 044023.

[24] Isabel Cordero-Carrion, José Marı´a Ibáñez, and Juan Antonio Morales-Lladosa. "Maximal slicings in spherical symmetry: local existence and construction". In: *Journal of mathematical physics* 52.11 (2011), p. 112501.

[25] Isabel Cordero-Carrión et al. "Excision scheme for black holes in constrained evolution formulations: Spherically symmetric case". In: *Physical Review D* 90.4 (2014), p. 044062.

[26] Isabel Cordero-Carrión et al. "Improved constrained scheme for the Einstein equations: An approach to the uniqueness issue". In: *Physical Review D* 79.2 (2009), p. 024017.

[27] Isabel Cordero-Carrión et al. "Mathematical issues in a fully constrained formulation of the Einstein equations". In: *Physical Review D* 77.8 (2008), p. 084007.

[28] Richard Courant, Kurt Friedrichs, and Hans Lewy. "Über die partiellen Differenzengleichungen der mathematischen Physik". In: *Mathematische annalen* 100.1 (1928), pp. 32–74.

[29] Harald Dimmelmeier, Jose A Font, and Ewald Müller. "Relativistic simulations of rotational core collapse II. Collapse dynamics and gravitational radiation". In: *Astronomy & Astrophysics* 393.2 (2002), pp. 523–542.

[30] Harald Dimmelmeier, Nikolaos Stergioulas, and José A Font. "Non-linear axisymmetric pulsations of rotating relativistic stars in the conformal flatness approximation". In: *Monthly Notices of the Royal Astronomical Society* 368.4 (2006), pp. 1609–1630.

[31] PAM Dirac. "Fixation of coordinates in the Hamiltonian theory of gravitation". In: *Physical Review* 114.3 (1959), p. 924.

[32] Lawrence C Evans. "Partial differential equations and Monge-Kantorovich mass transfer". In: *Current developments in mathematics* 1997.1 (1997), pp. 65–126.

[33] Filippo Galeazzi et al. "Implementation of a simplified approach to radiative transfer in general relativity". In: *Physical Review D* 88.6 (2013), p. 064009.

[34] Eric Gourgoulhon. *3+ 1 formalism in general relativity: bases of numerical relativity*. Vol. 846. Springer Science & Business Media, 2012.

[35] Ami Harten. "High resolution schemes for hyperbolic conservation laws". In: *Journal of computational physics* 135.2 (1997), pp. 260–278.

[36] Amiram Harten, Peter D Lax, and Bram van Leer. "On upstream differencing and Godunov-type schemes for hyperbolic conservation laws". In: *SIAM review* 25.1 (1983), pp. 35–61.

[37] Jan S Hesthaven and Tim Warburton. *Nodal discontinuous Galerkin methods: algorithms, analysis, and applications*. Springer Science & Business Media, 2007.

[38] Xiangyu Y Hu, Nikolaus A Adams, and Chi-Wang Shu. "Positivity-preserving method for high-order conservative schemes solving compressible Euler equations". In: *Journal of Computational Physics* 242 (2013), pp. 169–180.

[39] James A Isenberg. "Waveless approximation theories of gravity". In: *International Journal of Modern Physics D* 17.02 (2008), pp. 265–273.

[40] Rony Keppens et al. "MPI-AMRVAC: a parallel, grid-adaptive PDE toolkit". In: *Computers & Mathematics with Applications* 81 (2021), pp. 316–333.

[41] VP Kolgan. "Application of the minimum-derivative principle in the construction of finite-difference schemes for numerical analysis of discontinuous solutions in gas dynamics". In: *Uchenye Zapiski TsaGI [Sci. Notes Central Inst. Aerodyn]* 3.6 (1972), pp. 68–77.

[42] Godunov Sergei Konstantinovich. "A difference method for numerical calculation of discontinuous solutions of the equations of hydrodynamics". In: *Matematicheskii Sbornik* 89.3 (1959), pp. 271–306.

[43] Bram van Leer. "An introduction to the article "Reminiscences about difference schemes" by SK Godunov". In: *Journal of Computational Physics* 153.1 (1999), pp. 1–5.

[44] André Lichnerowicz. *L'intégration des équations de la gravitation relativiste et le problème des n-corps*. Gauthier-Villars, 1944.

[45] Barry Merriman. "Understanding the Shu–Osher conservative finite difference form". In: *Journal of Scientific Computing* 19.1 (2003), pp. 309–322.

[46] Charles W Misner, Kip S Thorne, and John Archibald Wheeler. *Gravitation*. Macmillan, 1973.

[47] Pedro J Montero, Thomas W Baumgarte, and Ewald Müller. "General relativistic hydrodynamics in curvilinear coordinates". In: *Physical Review D* 89.8 (2014), p. 084043.

[48] Bernhard Müller. "The dynamics of neutrino-driven supernova explosions after shock revival in 2D and 3D". In: *Monthly Notices of the Royal Astronomical Society* 453.1 (2015), pp. 287–310.

[49] Takashi Nakamura. "3D numerical relativity." In: *Relativistic Cosmology* (1994), pp. 155–182.

[50] Roland Oechslin, Stephan Rosswog, and Friedrich-Karl Thielemann. "Conformally flat smoothed particle hydrodynamics application to neutron star mergers". In: *Physical Review D* 65.10 (2002), p. 103005.

[51] Christian D Ott et al. "Rotating collapse of stellar iron cores in general relativity". In: *Classical and Quantum Gravity* 24.12 (2007), S139.

[52] AG Pili, N Bucciantini, and L Del Zanna. "Axisymmetric equilibrium models for magnetized neutron stars in General Relativity under the Conformally Flat Condition". In: *Monthly Notices of the Royal Astronomical Society* 439.4 (2014), pp. 3541–3563.

[53] AG Pili, NICCOLO' Bucciantini, and L Del Zanna. "General relativistic models for rotating magnetized neutron stars in conformally flat space–time". In: *Monthly Notices of the Royal Astronomical Society* 470.2 (2017), pp. 2469–2493.

[54] AG Pili, NICCOLO' Bucciantini, and L Del Zanna. "General relativistic neutron stars with twisted magnetosphere". In: *Monthly Notices of the Royal Astronomical Society* 447.3 (2015), pp. 2821–2835.

[55] William H Press et al. *Numerical recipes in Fortran 90: Volume 2, volume 2 of Fortran numerical recipes: The art of parallel scientific computing*. Cambridge university press, 1996.

[56] Murray H Protter and Hans F Weinberger. *Maximum principles in differential equations*. Springer Science & Business Media, 2012.

[57] Luciano Rezzolla and Olindo Zanotti. *Relativistic hydrodynamics*. Oxford University Press, 2013.

[58] Philip L Roe. "Characteristic-based schemes for the Euler equations". In: *Annual review of fluid mechanics* 18.1 (1986), pp. 337–365.

[59] Vladimir Vasil'evich Rusanov. *Calculation of interaction of non-steady shock waves with obstacles*. NRC, Division of Mechanical Engineering, 1962.

[60] Motoyuki Saijo. "The collapse of differentially rotating supermassive stars: conformally flat simulations". In: *The Astrophysical Journal* 615.2 (2004), p. 866.

[61] Masaru Shibata. *Numerical Relativity*. Vol. 1. World Scientific, 2015.

[62] Masaru Shibata and Takashi Nakamura. "Evolution of three-dimensional gravitational waves: Harmonic slicing case". In: *Physical Review D* 52.10 (1995), p. 5428.

[63] Masaru Shibata and Yu-ichirou Sekiguchi. "Gravitational waves from axisymmetric rotating stellar core collapse to a neutron star in full general relativity". In: *Physical Review D* 69.8 (2004), p. 084024.

[64] Masaru Shibata and Koji Uryū. "Merger of black hole-neutron star binaries: Nonspinning black hole case". In: *Physical Review D* 74.12 (2006), p. 121503.

[65] Chi-Wang Shu. "Total-variation-diminishing time discretizations". In: *SIAM Journal on Scientific and Statistical Computing* 9.6 (1988), pp. 1073–1084.

[66] Chi-Wang Shu and Stanley Osher. "Efficient implementation of essentially non-oscillatory shock-capturing schemes". In: *Journal of computational physics* 77.2 (1988), pp. 439–471.

[67] Chi-Wang Shu and Stanley Osher. "Efficient implementation of essentially non-oscillatory shock-capturing schemes, II". In: *Upwind and High-Resolution Schemes*. Springer, 1989, pp. 328–374.

[68] Larry L Smarr. *Sources of Gravitational Radiation: Proceedings of the Battelle Seattle Workshop*. CUP Archive, 1979.

[69] Larry Smarr and James W York Jr. "Radiation gauge in general relativity". In: *Physical Review D* 17.8 (1978), p. 1945.

[70] A Suresh and HT Huynh. "Accurate monotonicity-preserving schemes with Runge–Kutta time stepping". In: *Journal of Computational Physics* 136.1 (1997), pp. 83–99.

[71] Michael Eugene Taylor. *Partial differential equations. 3, Nonlinear equations*. Springer, 1991.

[72] Saul A Teukolsky. "Linearized quadrupole waves in general relativity and the motion of test particles". In: *Physical Review D* 26.4 (1982), p. 745.

[73] Jannis Teunissen and Ute Ebert. "Afivo: A framework for quadtree/octree AMR with shared-memory parallelization and geometric multigrid methods". In: *Computer Physics Communications* 233 (2018), pp. 156–166.

[74] Jannis Teunissen and Rony Keppens. "A geometric multigrid library for quadtree/octree AMR grids coupled to MPI-AMRVAC". In: *Computer Physics Communications* 245 (2019), p. 106866.

[75] Eleuterio F Toro. *Riemann solvers and numerical methods for fluid dynamics: a practical introduction*. Springer Science & Business Media, 2013.

[76] Ulrich Trottenberg, Cornelius W Oosterlee, and Anton Schuller. *Multigrid*. Elsevier, 2000.

[77] Bram Van Leer. "Towards the ultimate conservative difference scheme. II. Monotonicity and conservation combined in a second-order scheme". In: *Journal of computational physics* 14.4 (1974), pp. 361–370.

[78] Bram Van Leer. "Towards the ultimate conservative difference scheme. IV. A new approach to numerical convection". In: *Journal of computational physics* 23.3 (1977), pp. 276–299.

[79] Bram Van Leer. "Towards the ultimate conservative difference scheme. V. A second-order sequel to Godunov's method". In: *Journal of computational Physics* 32.1 (1979), pp. 101–136.

[80] James R Wilson and Grant J Mathews. "Relativistic hydrodynamics." In: *Frontiers in numerical relativity* (1989), pp. 306–314.

[81] C Xia et al. "MPI-AMRVAC 2.0 for solar and astrophysical applications". In: *The Astrophysical Journal Supplement Series* 234.2 (2018), p. 30.

[82] James W York Jr. "Conformally invariant orthogonal decomposition of symmetric tensors on Riemannian manifolds and the initial-value problem of general relativity". In: *Journal of Mathematical Physics* 14.4 (1973), pp. 456–464.

[83] James W York Jr. "Gravitational degrees of freedom and the initial-value problem". In: *Physical Review Letters* 26.26 (1971), p. 1656.

[84] James W York Jr. "Kinematics and dynamics of general relativity". In: *Sources of gravitational radiation* (1979), pp. 83–126.

[85] James W York Jr. "Role of conformal three-geometry in the dynamics of gravitation". In: *Physical review letters* 28.16 (1972), p. 1082.

[86] David M Young. *Iterative solution of large linear systems*. Elsevier, 2014.

[87] Weiqun Zhang et al. "Boxlib with tiling: An adaptive mesh refinement software framework". In: *SIAM Journal on Scientific Computing* 38.5 (2016), S156–S172.

[88] U Ziegler. "A semi-discrete central scheme for magnetohydrodynamics on orthogonal–curvilinear grids". In: *Journal of Computational Physics* 230.4 (2011), pp. 1035–1063.

Appendix A

Useful relations for implementation of constrained scheme

A.1 The elliptic equations in constrained scheme

We use orthonormal-basis for the vector fields and tensor fields in the elliptic equations in section 1.5.1 and 1.5.3. The expression and discretization of the equations in cylindrical and spherical coordinate is non-trival under orthonormal-basis. We list the relations in various geometry in the following.

A.1.1 Cylindrical coordinate

The scalar laplacian in cylindrical coordinate is given by

$$\mathcal{D}^2 u = \frac{1}{r}\frac{\partial}{\partial r}\left(r\frac{\partial u}{\partial r}\right) + \frac{1}{r^2}\frac{\partial^2 u}{\partial \phi^2} + \frac{\partial^2 u}{\partial z^2}, \tag{A.1}$$

while the corresponding discretization is given by

$$\begin{aligned}\mathcal{D}^2 u_{i,j,k} = &\frac{r_{i+1/2}\left(u_{i+1,j,k} - u_{i,j,k}\right) - r_{i-1/2}\left(u_{i,j,k} - u_{i-1,j,k}\right)}{r_i \Delta r^2} \\ &+ \frac{u_{i,j+1,k} - 2u_{i,j,k} + u_{i,j-1,k}}{r_i^2 \Delta \phi^2} + \frac{u_{i,j,k+1} - 2u_{i,j,k} + u_{i,j,k-1}}{\Delta z^2}.\end{aligned} \tag{A.2}$$

For a generic vector $\mathbf{X} = \left(X^r, X^\phi, X^z\right)$, its divergence is given by

$$\mathcal{D}_i X^i = \frac{1}{r}\frac{\partial\left(rX^r\right)}{\partial r} + \frac{1}{r}\frac{\partial X^\phi}{\partial \phi} + \frac{\partial X^z}{\partial z}, \tag{A.3}$$

and the vector laplacian is

$$\left(\Delta_L \mathbf{X}\right)^r = \mathcal{D}^2 X^r - \frac{2}{r^2}\frac{\partial X^\phi}{\partial \phi} + \frac{1}{3}\frac{\partial}{\partial r}\left(\mathcal{D}_i X^i\right), \tag{A.4}$$

$$\left(\Delta_L \mathbf{X}\right)^\phi = \mathcal{D}^2 X^\phi - \frac{X^\phi}{r^2} + \frac{2}{r^2}\frac{\partial X^r}{\partial \phi} + \frac{1}{3r}\frac{\partial}{\partial \phi}\left(\mathcal{D}_i X^i\right), \tag{A.5}$$

$$\left(\Delta_L \mathbf{X}\right)^z = \mathcal{D}^2 X^z + \frac{1}{3}\frac{\partial}{\partial z}\left(\mathcal{D}_i X^i\right). \tag{A.6}$$

The generalized Dirac gauge conditions in cylindrical coordinate is given by

$$\left(\mathcal{D}_j h^{ij}\right)^r = \mathcal{D}_j h^{rj} - \frac{h^{\phi\phi}}{r}, \tag{A.7}$$

$$\left(\mathcal{D}_j h^{ij}\right)^\phi = \mathcal{D}_j h^{\phi j} + \frac{h^{r\phi}}{r}, \tag{A.8}$$

$$\left(\mathcal{D}_j h^{ij}\right)^z = \mathcal{D}_j h^{zj}. \tag{A.9}$$

A.1.2 Spherical coordinate

The scalar laplacian in spherical coordinate is given by

$$\mathcal{D}^2 u = \frac{1}{r^2}\frac{\partial}{\partial r}\left(r^2\frac{\partial u}{\partial r}\right) + \frac{1}{r^2\sin\theta}\frac{\partial}{\partial \theta}\left(\sin\theta\frac{\partial u}{\partial \theta}\right) + \frac{1}{r^2\sin^2\theta}\frac{\partial^2 u}{\partial \phi^2} \tag{A.10}$$

while the corresponding discretization is given by

$$\begin{aligned}\mathcal{D}^2 u_{i,j,k} =& \frac{r_{i+1/2}^2\left(u_{i+1,j,k} - u_{i,j,k}\right) - r_{i-1/2}^2\left(u_{i,j,k} - u_{i-1,j,k}\right)}{r_i^2 \Delta r^2} \\ &+ \frac{\sin\theta_{j+1/2}\left(u_{i,j+1,k} - u_{i,j,k}\right) - \sin\theta_{j-1/2}\left(u_{i,j,k} - u_{i,j-1,k}\right)}{r_i^2\sin\theta_j \Delta\theta^2} \\ &+ \frac{u_{i,j,k+1} - 2u_{i,j,k} + u_{i,j,k-1}}{r_i^2\sin^2\theta_j \Delta\phi^2}.\end{aligned} \tag{A.11}$$

For a generic vector $\mathbf{X} = \left(X^r, X^\theta, X^\phi\right)$, its divergence is given by

$$\mathcal{D}_i X^i = \frac{1}{r^2}\frac{\partial\left(r^2 X^r\right)}{\partial r} + \frac{1}{r\sin\theta}\frac{\partial\left(\sin\theta X^\theta\right)}{\partial\theta} + \frac{1}{r\sin\theta}\frac{\partial X^\phi}{\partial\phi} \tag{A.12}$$

and the vector laplacian is

$$\left(\Delta_L \mathbf{X}\right)^r = \mathcal{D}^2 X^r - \frac{2}{r^2}\left[X^r + \frac{1}{\sin\theta}\frac{\partial\left(\sin\theta X^\theta\right)}{\partial\theta} + \frac{1}{\sin\theta}\frac{\partial X^\phi}{\partial\phi}\right] + \frac{1}{3}\frac{\partial}{\partial r}\left(\mathcal{D}_i X^i\right), \tag{A.13}$$

$$\left(\Delta_L \mathbf{X}\right)^\theta = \mathcal{D}^2 X^\theta + \frac{2}{r^2}\frac{\partial X^r}{\partial\theta} - \frac{X^\theta}{r^2\sin^2\theta} - \frac{2\cos\theta}{r^2\sin^2\theta}\frac{\partial X^\phi}{\partial\phi} + \frac{1}{3r}\frac{\partial}{\partial\theta}\left(\mathcal{D}_i X^i\right), \tag{A.14}$$

$$\left(\Delta_L \mathbf{X}\right)^\phi = \mathcal{D}^2 X^\phi - \frac{X^\phi}{r^2\sin^2\theta} + \frac{2}{r^2\sin\theta}\frac{\partial X^r}{\partial\phi} + \frac{2\cos\theta}{r^2\sin^2\theta}\frac{\partial X^\theta}{\partial\phi} + \frac{1}{3r\sin\theta}\frac{\partial}{\partial\phi}\left(\mathcal{D}_i X^i\right). \tag{A.15}$$

The generalized Dirac gauge conditions in spherical coordinate is given by

$$\left(\mathcal{D}_j h^{ij}\right)^r = \mathcal{D}_j h^{rj} - \frac{h^{\theta\theta} + h^{\phi\phi}}{r}, \tag{A.16}$$

$$\left(\mathcal{D}_j h^{ij}\right)^\theta = \mathcal{D}_j h^{\theta j} + \frac{h^{r\theta} - \cot\theta h^{\phi\phi}}{r}, \tag{A.17}$$

$$\left(\mathcal{D}_j h^{ij}\right)^\phi = \mathcal{D}_j h^{\phi j} + \frac{h^{r\phi} + \cot\theta h^{\theta\phi}}{r}. \tag{A.18}$$

Appendix B

Reference flat metric in 3D

Appendix C

Analytic Solution of Teukolsky Wave

We list here the analytic solution of Teukolsky wave in 2D cylindrical coordinate with the initial condition writen in equations 4.17

$$
\begin{aligned}
h^{rr}(r,z,t) = -\frac{1}{8\lambda^8 R^9}\Bigg[& 3\mathcal{A}' e^{-\frac{(R+t)^2}{\lambda^2}}(80\lambda^2 r^2 R^2 t z^2 \\
& (-R^4(e^{\frac{4Rt}{\lambda^2}}-1) - 3R^2t^2(e^{\frac{4Rt}{\lambda^2}}-1) + 3R^3 t \\
& (e^{\frac{4Rt}{\lambda^2}}+1) + Rt^3(e^{\frac{4Rt}{\lambda^2}}+1)) + 16r^2R^4z^2(-10R^2t^3 \\
& (e^{\frac{4Rt}{\lambda^2}}-1) + t^2((10R^3 - t^3)e^{\frac{4Rt}{\lambda^2}} + 10R^3 \\
& + t^3) + R^4((R-5t)e^{\frac{4Rt}{\lambda^2}} + R + 5t) + 5Rt^4(e^{\frac{4Rt}{\lambda^2}}+1)) \\
& + 3\lambda^8 t(4r^4 - 27r^2z^2 + 4z^4)(e^{\frac{4Rt}{\lambda^2}}-1) - 4\lambda^4R^2(-t^3 \\
& (4r^4 - 37r^2z^2 + 4z^4)(e^{\frac{4Rt}{\lambda^2}}-1) + 3Rt^2(4r^4 - 17r^2z^2 + 4z^4) \\
& (e^{\frac{4Rt}{\lambda^2}}+1) - 6t(2r^6 + r^4z^2 + r^2z^4 + 2z^6)(e^{\frac{4Rt}{\lambda^2}}-1) \\
& + 4R^7(e^{\frac{4Rt}{\lambda^2}}+1)) - 6\lambda^6 t(-4r^6(e^{\frac{4Rt}{\lambda^2}}-1) \\
& + r^4(4Rt(e^{\frac{4Rt}{\lambda^2}}+1) + 13z^2(e^{\frac{4Rt}{\lambda^2}}-1)) \\
& + r^2z^2(13z^2(e^{\frac{4Rt}{\lambda^2}}-1) - 27Rt(e^{\frac{4Rt}{\lambda^2}}+1)) \\
& - 4z^6(e^{\frac{4Rt}{\lambda^2}}-1) + 4Rtz^4(e^{\frac{4Rt}{\lambda^2}}+1)))\Bigg],
\end{aligned}
\tag{C.1}
$$

$$
\begin{aligned}
h^{rz}(r,z,t) = \frac{1}{8\lambda^8 R^9}\Bigg[& 3r\mathcal{A}' z e^{-\frac{(R+t)^2}{\lambda^2}}(16r^2R^4(-10R^2t^3(e^{\frac{4Rt}{\lambda^2}}-1) \\
& + t^2((10R^3-t^3)e^{\frac{4Rt}{\lambda^2}}+10R^3+t^3)+R^4((R-5t)e^{\frac{4Rt}{\lambda^2}}+R+5t)+5Rt^4(e^{\frac{4Rt}{\lambda^2}}+1)) \\
& + 15\lambda^8 t(4z^2-3r^2)(e^{\frac{4Rt}{\lambda^2}}-1)+12\lambda^4R^2t(t^2(8z^2-7r^2)(e^{\frac{4Rt}{\lambda^2}}-1) \\
& + Rt(9r^2-16z^2)(e^{\frac{4Rt}{\lambda^2}}+1)-2(r^4-3r^2z^2-4z^4)(e^{\frac{4Rt}{\lambda^2}}-1)) \\
& - 16\lambda^2R^2(-R^4t(3r^2+8z^2)(e^{\frac{4Rt}{\lambda^2}}-1)+Rt^4(2z^2-3r^2)(e^{\frac{4Rt}{\lambda^2}}+1) \\
& + t^3(7r^4-r^2z^2-8z^4)(e^{\frac{4Rt}{\lambda^2}}-1)-3Rt^2(r^4-3r^2z^2-4z^4)(e^{\frac{4Rt}{\lambda^2}}+1) \\
& + 2R^7(e^{\frac{4Rt}{\lambda^2}}+1))-6\lambda^6t(9r^4(e^{\frac{4Rt}{\lambda^2}}-1)-15r^2Rt(e^{\frac{4Rt}{\lambda^2}}+1) \\
& + z^2(20Rt(e^{\frac{4Rt}{\lambda^2}}+1)-7r^2(e^{\frac{4Rt}{\lambda^2}}-1))-16z^4(e^{\frac{4Rt}{\lambda^2}}-1)))\Bigg],
\end{aligned}
\tag{C.2}
$$

$$
h^{r\phi}(r,z,t) = 0, \tag{C.3}
$$

$$
\begin{aligned}
h^{zz}(r,z,t) = -\frac{1}{8\lambda^8 R^9}\Bigg[& 3\mathcal{A}' e^{-\frac{(R+t)^2}{\lambda^2}}(16r^4R^4(-10R^2t^3(e^{\frac{4Rt}{\lambda^2}}-1) \\
& + t^2((10R^3-t^3)e^{\frac{4Rt}{\lambda^2}}+10R^3+t^3)+R^4((R-5t)e^{\frac{4Rt}{\lambda^2}}+R+5t)+5Rt^4(e^{\frac{4Rt}{\lambda^2}}+1)) \\
& - 16\lambda^2r^2R^2(-R^4t(11r^2+16z^2)(e^{\frac{4Rt}{\lambda^2}}-1)-Rt^4(r^2-4z^2)(e^{\frac{4Rt}{\lambda^2}}+1) \\
& - t^3(r^4+17r^2z^2+16z^4)(e^{\frac{4Rt}{\lambda^2}}-1)+3Rt^2(3r^4+11r^2z^2+8z^4)(e^{\frac{4Rt}{\lambda^2}}+1) \\
& + 4R^7(e^{\frac{4Rt}{\lambda^2}}+1))-3\lambda^8t(3r^4-24r^2z^2+8z^4)(e^{\frac{4Rt}{\lambda^2}}-1) \\
& + 4\lambda^4R^2(-t^3(5r^4-32r^2z^2+8z^4)(e^{\frac{4Rt}{\lambda^2}}-1)+3Rt^2(r^4-16r^2z^2+8z^4)(e^{\frac{4Rt}{\lambda^2}}+1) \\
& - 6t(r^6+r^4z^2+4r^2z^4+4z^6)(e^{\frac{4Rt}{\lambda^2}}-1)+8R^7(e^{\frac{4Rt}{\lambda^2}}+1))+6\lambda^6t(-(r^6(e^{\frac{4Rt}{\lambda^2}}-1)) \\
& + 3r^4Rt(e^{\frac{4Rt}{\lambda^2}}+1)+8z^4(r^2(e^{\frac{4Rt}{\lambda^2}}-1)+Rt(e^{\frac{4Rt}{\lambda^2}}+1)) \\
& + 3r^2z^2(5r^2(e^{\frac{4Rt}{\lambda^2}}-1)-8Rt(e^{\frac{4Rt}{\lambda^2}}+1))-8z^6(e^{\frac{4Rt}{\lambda^2}}-1)))\Bigg],
\end{aligned}
\tag{C.4}
$$

$$
h^{z\phi}(r,z,t) = 0, \tag{C.5}
$$

$$
\begin{aligned}
h^{\phi\phi}(r,z,t) = \frac{1}{8\lambda^8 R^7}\Bigg[& 3\mathcal{A}' e^{-\frac{(R+t)^2}{\lambda^2}}(-16\lambda^2 r^2 R^2(-11R^4 t(e^{\frac{4Rt}{\lambda^2}}-1) \\
& - R^2 t^3(e^{\frac{4Rt}{\lambda^2}}-1) + 9R^3 t^2(e^{\frac{4Rt}{\lambda^2}}+1) + 4R^5(e^{\frac{4Rt}{\lambda^2}}+1) \\
& - Rt^4(e^{\frac{4Rt}{\lambda^2}}+1)) + 16r^2 R^4(-10R^2 t^3(e^{\frac{4Rt}{\lambda^2}}-1) + t^2((10R^3 - t^3)e^{\frac{4Rt}{\lambda^2}} \\
& + 10R^3 + t^3) + R^4((R-5t)e^{\frac{4Rt}{\lambda^2}} + R + 5t) + 5Rt^4(e^{\frac{4Rt}{\lambda^2}}+1)) + 3\lambda^8 t(r^2 - 4z^2) \\
& (e^{\frac{4Rt}{\lambda^2}}-1) + 4\lambda^4 R^2(-3Rt^2(3r^2-4z^2)(e^{\frac{4Rt}{\lambda^2}}+1) - t(-6r^4 + r^2(t^2+6z^2) + 4z^2(t^2+3z^2)) \\
& (e^{\frac{4Rt}{\lambda^2}}-1) + 4RR^4(e^{\frac{4Rt}{\lambda^2}}+1)) + 6\lambda^6 t(3r^4(e^{\frac{4Rt}{\lambda^2}}-1) \\
& - r^2(Rt(e^{\frac{4Rt}{\lambda^2}}+1) + z^2(e^{\frac{4Rt}{\lambda^2}}-1)) - 4z^4(e^{\frac{4Rt}{\lambda^2}}-1) \\
& + 4Rtz^2(e^{\frac{4Rt}{\lambda^2}}+1)))\Bigg],
\end{aligned}
\tag{C.6}
$$

where $R = \sqrt{r^2+z^2}$.